E. van Twist

The area of a unipolar electrogram to identify the arrhythmogenic substrate.

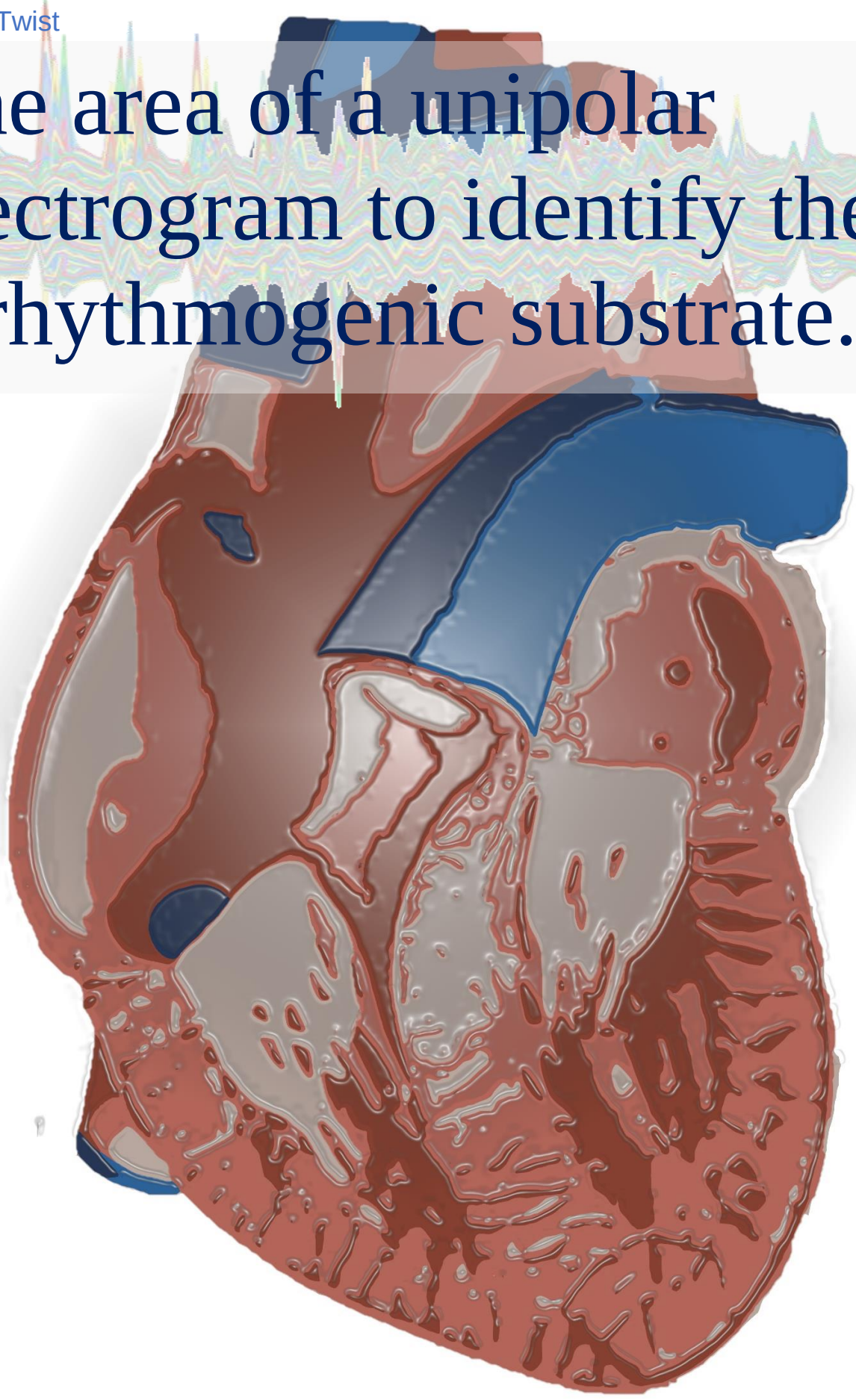

The area of a unipolar electrogram to identify the arrhythmogenic substrate.

E. van Twist
Student number: 4450965
September 2021

in partial fulfilment of the requirements for the joint degree of Master of Science in

Technical Medicine

Leiden University | Delft University of Technology | Erasmus University Rotterdam

Master thesis project (TM30004 ; 35 ECTS)

Dept. of Biomechanical Engineering, TUDELFT
Supervisor(s):
Prof.dr. N.M.S. de Groot
Dr.ir. R.C. Hendriks

Thesis committee members:

Prof.dr. N.M.S. de Groot (chair)
Dr.ir. R.C. Hendriks
Dr. Y.J.H.J. Taverne
drs. M.S. van Schie

Preface

Before you lies my graduation thesis, containing the result of research conducted on the department of Translational Electrophysiology & Cardiology at Erasmus Medical Centre from April – September 2021. With this research I'm able to fulfil the graduation requirements of the joint Master degree Technical Medicine.

A mere six years ago I embarked on this journey, as part of only the second cohort of the bachelor program Clinical Technology. Applying had been a last-minute decision, yet I had never felt so destined for a program before. And so I worked very hard, first during my secondary school exams to bypass the bachelor selection procedure and then throughout my bachelors to graduate nominally in 2018. During my masters I began to experience doubt for the first time: what if present-day clinicians weren't ready for this new expertise? But over time I've seen the hospital-wide added value and contributions of Technical Physicians in clinical innovation, in implementation and in research.

I conducted my first clinical internship at the same department as my graduation thesis, working on a research project about atrial fibrillation using artificial intelligence algorithms. Cardiology has always been a field of intrigue. On the department, Technical Medicine was well known and there were even two Technical Physicians conducting a PhD here. For the first time I saw a smooth mixing of medicine and technology in research. Since then I knew that I wanted to conduct my graduation thesis here. My second internship was at the heart-lung centre in Leiden. After a few weeks the internship was postponed until further notice due to the pandemic. During this period I partook in Operation AIR, a non-profit student organization dedicated to the design of a pandemic ventilator to combat an expected shortage in ventilation systems on the intensive care departments. With this initiative we were able to demonstrate the essence of Technical Medicine. Multiple ventilators were successfully produced and remain in storage at the Ministry of Health. My final clinical internship was at the department of Neonatology, where I found my calling and true passion, working with data-monitoring in infants and children.

Now that my time as a student is coming to an end, everything appears to fall into place. In November I will start as a Technical Physician on the paediatric intensive care unit at Sophia Kinderziekenhuis, Erasmus MC. I am beyond excited to graduate and start this new journey. Sometimes it feels like it was written in the stars. Maybe a quote I came across here at the department is most suitable to describe it: *"I'm realistic. I expect miracles."*

E. van Twist
Rotterdam, October 2021

Contents

List of Abbreviations

AF	Atrial fibrillation
SR	Sinus rhythm
(U-)EGM	(Unipolar) electrogram
EA	Electrogram area
MVD	Mitral valve disease
SAN	Sinus-atrial node
AVN	Atrio-ventricular node
ECG	Electrocardiography
RA	Right atrium
LA	Left atrium
BB	Bachmann's Bundle
PV	Pulmonary veins
VF	Ventricular fibrillation
LAT	Local activation time

Abstract

Background: Unipolar electrograms (U-EGMs) contain additional information about interatrial activation and conduction in their morphology, which may aid towards improved diagnosis and staging of atrial fibrillation (AF).
Objective: The primary objective is to investigate regional differences in electrogram area (EA) during SR and AF and to design a patient-specific EA fingerprint, to characterize the arrhythmogenic substrate in patients with mitral valve disease (MVD).
Methods: Patients (N = 42) either with ('AF group', N = 23) or without a history of AF ('No AF group', N = 19), undergoing elective open heart surgery underwent high-resolution mapping of the right atrium (RA), left atrium (LA) and pulmonary veins (PV) including Bachmann's bundle (BB). Spatial distributions of mean EA, variance and total EA were determined in SR and AF. Absolute EA values were correlated with amplitude, an established metric in substrate mapping.
Results: A total of 3104460 EAs were analysed and compared between rhythms, regions and groups (Table 3). EA was larger in AF [SR: 54.97 (42.87), AF: 57.03 (51.02), $p < 0.01$], but smaller per region except the RA. In patients with AF, EA was significantly smaller across all atrial regions. During AF, amplitude showed moderate correlation with EA at best [no AF: $r = 0.54$ vs. AF: $= 0.51$].
Conclusion: The EA feature, entailing the U-EGM amplitude, duration and overall morphology, is suitable in signal fingerprinting to characterize the arrhythmogenic substrate and contains additional information compared with amplitude alone. Further studies are required to fine-tune the EA and implement EA-based classification.

Acknowledgements

I would like to express my sincere appreciation to my supervisors for their continued support and effort throughout this thesis. Natasja, thank you for handing me this project and believing that I could contribute to it. You are and have always been a true role model, especially for a female in this world. Richard, thank you for inviting me into the science of electro-technology and asking critical questions when needed. I always enjoyed showing you my results, your positive attitude is greatly appreciated. Mathijs, thank you for taking on the burden of being a daily supervisor and challenging me for continuous improvement. I would also like to thank Maarten, for his continued interest in my research (and for the delicious cups of tea). Participation of the entire department of Translation Electrophysiology & Cardiology is also greatly appreciated. Over time I've had many fruitful (and fun!) discussions, and I thank you all for that. Plus, you were willing to watch the Euro Cup with me during workhours, that was fun.

Appreciation also goes out to my family and friends, who have supported me continuously. Tara (and Taco, my cat), you always helped me to relieve my stress. You are not familiar with the medical field, yet I could always speak volumes to you about my thesis and I appreciate that. To my parents and sweet aunt Maaike, I know you don't really understand what I'm researching half of the time, but you're the biggest cheerleaders I've ever had and your pride is what drives me. Thank you, sincerely.

1. Introduction

Atrial fibrillation (AF) is the most common cardiac arrhythmia with high-risk of comorbidity and mortality, yet the arrhythmogenic substrate remains subject of research (1-4). Signal fingerprinting is a novel tool in substrate mapping to aid towards improved diagnostics and staging of AF, by constructing individualized electrical signal profiles (5). Fingerprints based on voltage and quantified morphological characteristics have been studied, but only during SR and generally reporting extensive inter-individual variations (6-8).

Substrate mapping comprises high-resolution intraoperative mapping to accurately measure electrical activity in the atria (9-11). Unipolar electrograms (U-EGMs) are increasingly used in substrate mapping, since they are independent of electrode position and wavefront direction (8, 12). U-EGMs contain information about interatrial activation and conduction in their morphology, which is effectively filtered out in the bipolar configuration. This information may aid towards improved diagnostics and staging of AF (13-15). The U-EGM morphology is determined by its amplitude, duration and RS-ratio, all of which are summarized by its area. The electrogram area (EA) can therefore be used to create representative EA profiles in the atria. Such EA fingerprints can reflect on morphological characteristics of unipolar potentials and provide a proxy of the spatial distribution of electric charge in the atria. Recently, Mendonca Costa et al. found that the absolute area of a bipolar electrogram normalized to the signal amplitude is a novel metric of local conduction delay, and could therefore have utility in substrate mapping procedures (16). However, this is not surprising since the bipolar electrogram is inherently dependent on wavefront propagation speed (17). Hence, additional research with the unipolar electrode configuration is required.

The goal of the present study, in a step towards the construction of an individualized AF fingerprint, is to construct unipolar EA-based measures of charge during SR and during AF to characterize electropathology and to investigate the effect of AF episodes in patients with mitral valve disease.

2. Background

2.1. Atrial fibrillation

Atrial fibrillation (AF) is the most common cardiac rhythm disorder (1, 2). It is estimated that by 2060, 17.9 million people will suffer from this condition in Europe alone (2). AF occurs when normal sinus rhythm (SR) is replaced by uncontrolled and chaotic electrical activity (1-3). The risk of overall mortality increases by nearly two-fold, while the risk of stroke increases by nearly five-fold (1-4). However, its pathophysiology remains incompletely understood and to date there is no curative therapy.

Contraction of the heart is triggered by electrical activation. In normal SR, excitation starts in the sinus-atrial node (SAN), the heart's physiological pacemaker, and is transmitted via the atrio-ventricular node (AVN) to the His-Purkinje fibers (Fig. 1) (18). In AF, electrical excitation occurs random and independently, causing simultaneous depolarization of independent areas throughout the atria (Fig. 1). This results in an irregular and often rapid heartbeat, with ineffective atrial contractions. The diagnosis AF is made when AF is recorded during a surface electrocardiogram (ECG). The ECG typically exhibits a lack of P-waves and irregularity of PR-intervals (Fig. 1) (19, 20).

Figure 1

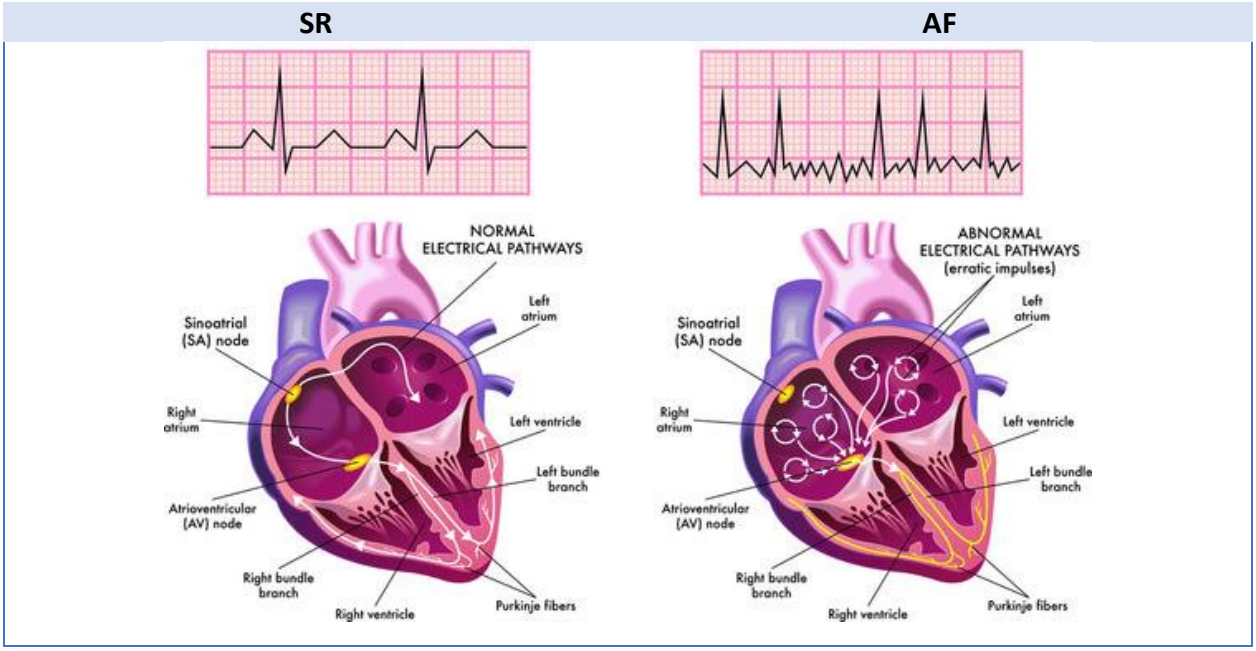

Schematic overview of the cardiac conduction system in normal sinus rhythm and in atrial fibrillation, with the corresponding rhythm recorded in an electrocardiogram. Figure borrowed from Adobe Stock.[1]

While AF onset requires a trigger, such as ectopic foci or re-entry circuits, maintenance and progression of AF requires a substrate (Fig.2) (21-23). Progression of AF occurs through structural damage and cardiac remodeling (19-25). Currently, AF is classified according to the possibility to intervene as either paroxysmal (lasting < 7 days and self-terminating), persistent (lasting > 7 days and not self-terminating) or permanent (cannot be terminated by medical intervention) (Fig. 2) (21, 26, 27). Initially, AF may go unnoticed when it is asymptomatic. Since diagnosis is ECG-based, there is often a delay between disease onset and actual diagnosis. During this time period, an arrhythmogenic substrate may already be formed (28). Current therapeutic modalities include electric cardioversion, anti-arrhythmic drugs and/or ablation (27-29). Their common denominator is that neither of them offers curation. In fact, progression of AF coexists with increased recurrence (29).

Figure 2

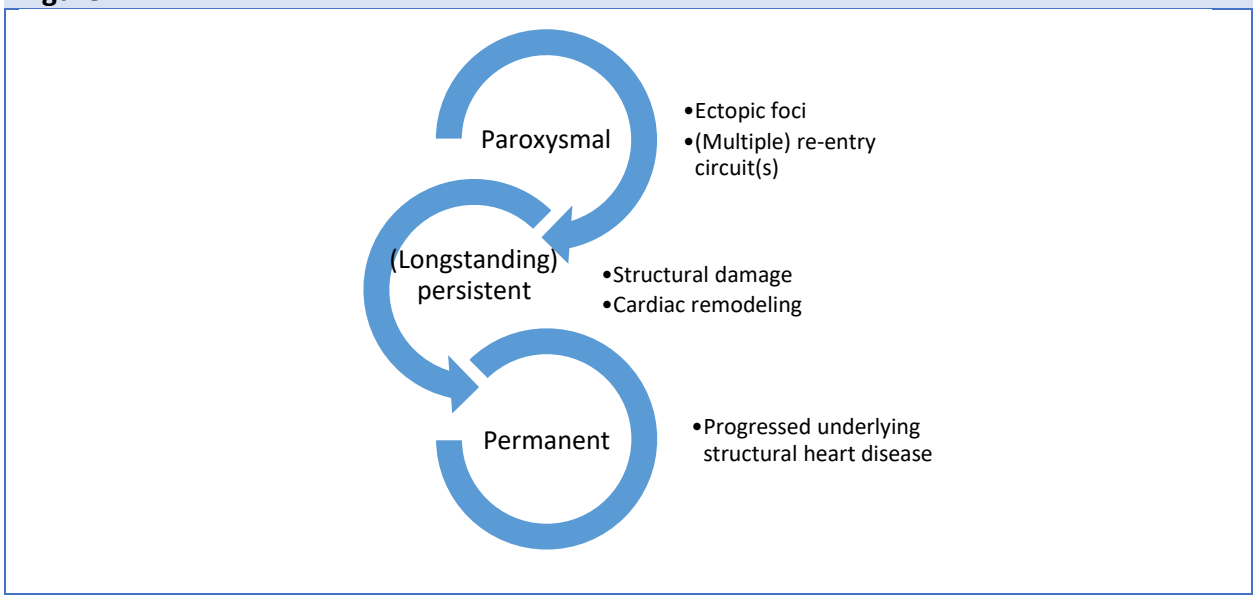

Schematic overview of progression of AF through trigger and substrate mechanism over time.

[1] Adobe Stock, via https://stock.adobe.com/sk/search/images?k=atrial+fibrillation+ecg&asset_id=318045353

2.2. High resolution intraoperative mapping

In epicardial mapping ('mapping'), arrays of 128- or 192-electrodes measure electrical activity directly from the myocardial surface during open heart surgery (9-11). Electric activation of cardiac tissue creates a propagating wave front (Fig. 3) (17). Excitation increases the negative membrane potential of resting cells through an influx of positively charged ions (17, 30). The gradient between active and resting tissue drives a transmembrane current that eventually returns via newly opened sodium channels (Fig. 3). This gives a positive extracellular field potential ahead of the wave front, and a negative potential behind it (17). By measuring transmembrane currents, the epicardial signal reflects the spatiotemporal distribution of myocardial electric potentials near the electrode.

The record of changes in electric potential of cells surrounding an electrode is known as the electrogram (EGM) (12, 31). In a unipolar electrode configuration, the epicardial signal is measured relative to a remote electrode (17). This provides an accurate measurement of local electrical activity and arrhythmogenicity with an omnidirectional field of view (12, 13). The unipolar EGM (U-EGM) can thus be seen as the sum of all per cell action potentials generated by a wavefront surrounding the recording electrode (8, 12, 13, 17). The measured signal is biphasic: positive as the wavefront approaches the electrode, zero when directly below the electrode and negative when it moves away (14, 15, 32). In the bipolar electrode configuration, the epicardial signal is obtained as the difference between two electrodes on a site of interest. (17) The signal is dependent on wavefront direction and on electrode position, orientation and sizing. (12, 13, 17) When a wavefront is at an unequal distance from the electrode pair, the bipolar EGM will be a function of the temporal offset between the electrodes (13, 17). In spite of the disadvantages, bipolar EGMs are frequently used in clinical practice because of the filtering effect of subtraction. Nonetheless, U-EGMs are now increasingly valued in research because of extra information contained in their morphology (12, 15, 17, 33).

The amplitude of U-EGMs reflects on the volume of tissue that is activated simultaneously. Low-voltages are associated with asynchronous activity, and nowadays increasingly used to define the AF substrate in voltage-guided ablation (8, 11, 17, 34). However, low-voltages are in part morphology-dependent (6, 15). A typical biphasic U-EGM morphology reflects homogenous conduction in tissue, while fractionation of EGMs reflects tissue with heterogeneous conduction (33, 35). In fractionation, the typical RS-wave of the EGM are replaced by multiple positive and negative peaks (33). Classification of RS-waves in SR has led to established association with atrial regions and inter-atrial conduction disorders (6).

Epicardial mapping has been used extensively in AF research to describe the arrhythmogenic substrate (36-38). The current focus is on the development of AF fingerprints, patient-specific profiles containing electrophysiological markers. The concept was introduced in an ongoing study by Starreveld et al., who hypothesized that AF fingerprints are unique for individual patients and dependent on age, gender and underlying heart disease (5). Van Schie et al., constructed unipolar voltage fingerprints to identify low-voltage areas and study the effects of AF, but reported large intra- and inter-patient variations (8). Ye et al., combined quantified features of morphology into a fingerprint and concluded that this may serve as a diagnostic tool to determine the severity and extensiveness of conduction inhomogeneity (7).

Figure 3

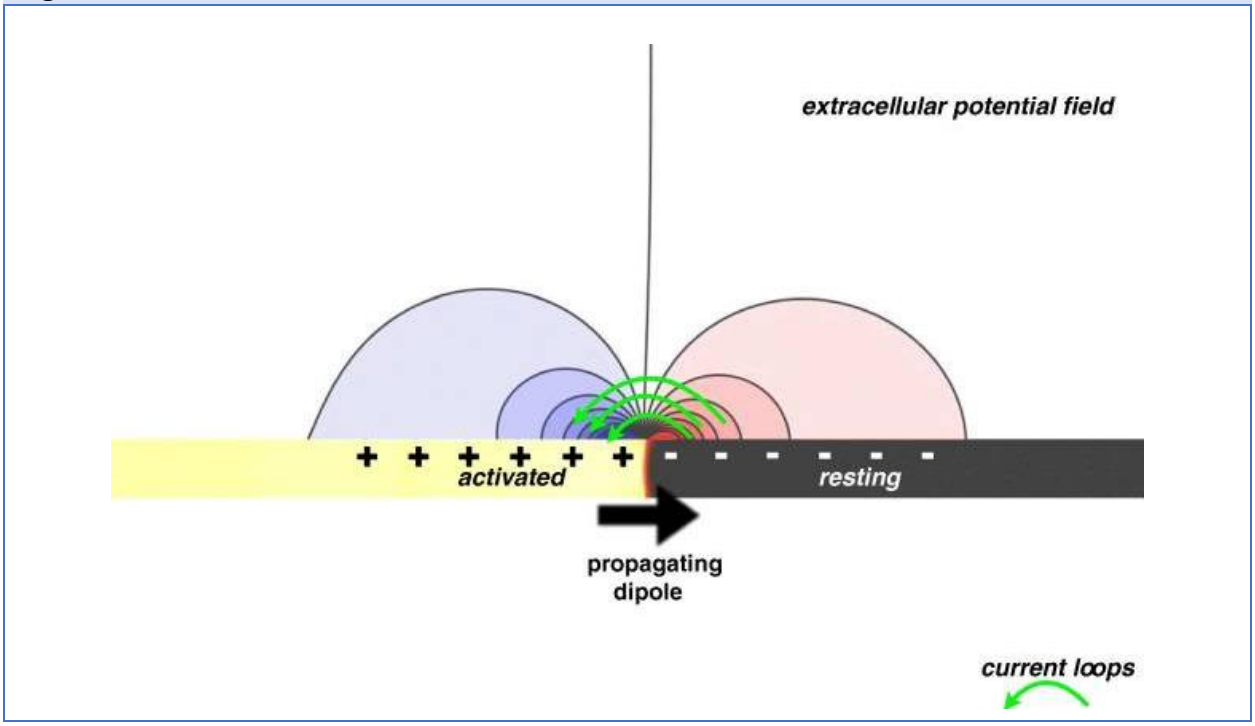

Representation of the extracellular field created by an activation wave-front as a propagating dipole. Figure borrowed from Sim et al. (20).

2.3. Problem statement

A suitable feature for signal fingerprinting is the area below an U-EGM. As stated prior, U-EGMs contain additional information about interatrial activation and conduction in their morphology, which may be obtained through EA. (6, 7) Essentially, EA entails a combination of amplitude, duration and overall morphology. Signal amplitude is an established metric in substrate mapping. However, large intra- and interpatient variations complicate its use to describe individual electropathology. It is expected that EA provides a more robust measure of arrhythmogenicity. Recently, Mendonca Costa et al. found a linear relation between the amplitude-normalized area of a bipolar EGM and the level of local conduction delay in tachyarrhythmias. They found that the EA increased in spite of a reduction in amplitude (16).

EA is obtained as the integral of an EGM. An EGM can mathematically be represented as: (31)

$$\Phi(y,t) = \frac{1}{4\pi\sigma_e}\int \frac{I_m(x,t)}{||y-x||}dA(x) \quad (1)$$

where y is the cell location, x the electrode location, t the time, σ_e the extracellular conductivity, I_m the transmembrane current and A the area measured by the electrode. Mathematical integration of an EGM then produces Eq. 2, where the independent limits of the integral can be interchanged to get Eq. 3:

$$\int \Phi(y,t)dt = \frac{1}{4\pi\sigma_e}\int\int \frac{I_m(x,t)}{||y-x||}dA(x)\,dt(t) \quad (2)$$

$$\int \Phi(y,t)dt = \frac{1}{4\pi\sigma_e}\int\int \frac{I_m(x,t)}{||y-x||}dt(t)dA(x) \quad (3)$$

In (3) the transmembrane current in Ampere (A) is integrated over time in seconds (s), which is the formula for electric charge Q in Coulomb (C or A/s) as given by:

$$Q(x) = \int I_m(x,t)dt \quad (4)$$

The EA is thus a measure of electric charge in the cells surrounding an electrode. In epicardial mapping, determining the EA for all EGMs per electrode reveals the spatiotemporal distribution of charge in the atria, and the degree of heterogeneity in EGMs inter- and intra-electrode(s). As described by Hodgkin and Huxley in 1952, both excitation and conduction depend on the displacement of charged particles (30). Little is known about the distribution of electric charge in the atria. Yet, mapping has shown that critical AF sites are plagued by heterogeneity in electrical activation and conduction (39-43). This will likely impact electric charge. Research has shown an altered charge density across the cell membrane during ventricular fibrillation in canine hearts (44). A similar difference in charge is expected to exist between SR and AF.

There are some considerations regarding the calculation of the EA. Firstly, electric charge is the integral of current over time, but integration of EGMs produces an integral of potential over time. Although this potential is a model for the transmembrane currents, it requires additional scaling for cardiac tissue resistance by Ohm's Law. However, the assumption is made that this resistance is negligible and uniform throughout the atria (45). Secondly, the limits of the integration need to be determined. We opted to define the limits as the start- and endpoints of EGMs. This requires baseline wander correction and calculation of an error margin to roughly detect these points. The drawback is that final calculations are thus subjected to an error margin as well. But, in light of the current thesis and its context, we expect this error to be negligible and, most importantly, a constant.

One way to evaluate EA as a feature in AF fingerprinting is to analyze sufficient epicardial signals recorded during SR and AF and subsequently display the spatiotemporal distributions of EA. Comparing outcomes between rhythms, atrial regions and patients provides information about EA and electropathology.

2.4. Goal of the research

Fingerprints for characterizing electropathology in AF described by Starreveld et al., van Schie et al. and Ye. et al., offer a first approach to patient-tailored diagnosis and staging of AF. In order for the fingerprint to succeed, more eligible features need to be studied. The main goal of this thesis is:

> *To construct high-resolution unipolar EA-based measures of charge during SR and AF to characterize electropathology and to study the effect of AF episodes in patients with mitral valve disease.*

Subgoals of this thesis are:

- To research the relation between EA, amplitude and signal morphology;
- To research the relation between electric charge, atrial conductivity and electropathology;
- To write an algorithm that implements the mathematical integration of EGMs per electrode;
- To create a map that reveals the spatiotemporal distribution of electric charge in the atria;
- To validate findings using existing mapping studies and conductivity theorems.

We hypothesize that EA is a suitable feature to identify the arrhythmogenic substrate in fingerprinting. Loss of conductive properties in AF is expected to results in a larger EA via prolonged U-EGM duration, given that this effect is stronger than the reduction in amplitude and hence, the EA is superior to the latter.

3. Method

3.1. Data acquisition

3.1.1. Study population

This retrospective study was conducted using epicardial mapping data from an existing database containing patients with mitral valve disease. Epicardial mapping in these patients was conducted during elective open heart surgery in the Erasmus Medical Center Rotterdam from 2012 to present. Patient characteristics were obtained from medical records. Patients were classified as either with a history of AF (AF group) or without a history of AF (no AF group).

3.1.2. Intraoperative mapping procedure

High-resolution intraoperative mapping was performed prior to commencement of extra-corporal circulation, as previously described in detail (9-11, 39). A temporal bipolar epicardial pacemaker wire was attached to the right atrial free wall to serve as reference electrode. A steel wire fixed in the thoracic cavity served as indifferent electrode. Epicardial mapping was performed with 128- or 192-unipolar electrode arrays (electrode diameters 0.45 or 0.65 mm respectively, inter-electrode distance 2.0 mm). The atria were mapped according to the predefined scheme illustrated in Figure 4. The electrode arrays were shifted along imaginary lines, with a fixed anatomical orientation. This region covers the right (RA) and left atrium (LA), Bachman's Bundle (BB) and pulmonary veins (PV). Potentially there was some overlap in mapping to avoid omission of areas.

For all mapping sites, five seconds of SR and ten seconds of AF were recorded, including a calibration signal (2 mV, 1000 ms), surface electrocardiogram, bipolar reference EGM and all unipolar epicardial EGMs. In patients who presented in SR, AF was induced by programmed electrical stimulation (PES). In patients who presented in AF, SR was restored by cardioversion. Before storage on a hard disk, data were amplified (gain 1000), filtered (0.5-400 Hz), sampled (1 kHz) and converted from analogue to digital (16 bits).

Figure 4

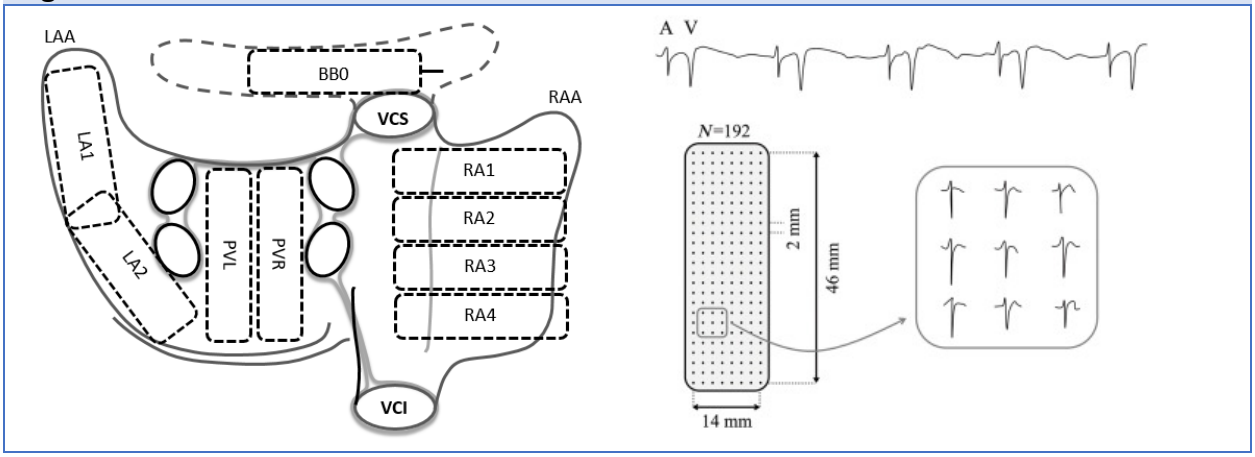

Schematic overview of mapping procedure. The left panel displays a posterior view of the atria, with projections of the 192-electrode array. The right panel displays a SR recording, with atrial (A) and far-field ventricular (V) deflections. Typical EGM morphologies are also depicted. LA = left atrium, LAA = left atrial appendage, PVL = left pulmonary vein, PVR = right pulmonary vein, RA = right atrium, RAA = right atrial appendage, SR = sinus rhythm, VCS = vena cava superior, VCI = vena cava inferior

3.2. Data analysis

3.2.1. Preprocessing

Unipolar EGMs were semi-automatically analyzed in custom software to construct activation maps (Fig. 5). Excluded from annotation were EGMs with injury potentials, recording sites with ≥25% excluded or missing EGMs and premature atrial complexes or aberrant beats. Far-field ventricular potentials were annotated as exclusion windows. The steepest negative slope of an atrial deflection was annotated as the local activation time (LAT), given that its amplitude was ≥ 2 the signal-to-noise ratio (SNR) of the U-EGM. The latency (minimal time between two consecutive deflections) was fixed at 2 ms. Patient recordings were eligible for inclusion in EA analysis if the epicardial signals were of sufficient quality and if both AF and SR recordings of at least one atrial location were available for comparison.

Figure 5

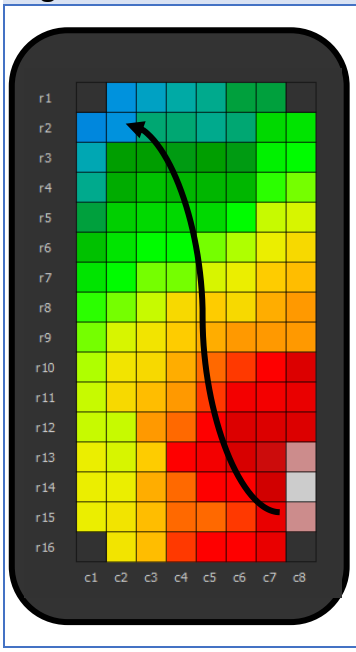

Exemplary wave front activation map. Colors reflect the electrode LAT. Here, the wavefront follows the direction of the arrow.

3.2.2. Baseline determination and baseline wander correction

The atrial vibrations in AF typically result in baseline wander of recorded epicardial signals. To correct for this wander, a baseline signal was established. We assumed that the baseline is the epicardial signal in-between consecutive EGMs. In a first approach, the baseline was defined iteratively per EGM as the interval $LAT - 100\ ms$ to $LAT - 30\ ms$ i.e. the epicardial signal before the EGM. This baseline was then low-pass filtered and interpolated through the EGM. However, in a second attempt we opted for a more uniform approach (Fig. 6). All atrial and far-field ventricular potentials were cut from the epicardial signal with the aid of a fixed window between two consecutive LATs ($LAT_1 + 10\ ms$ to $LAT_2 - 20\ ms$) and a boolean index. The remaining inter-EGM epicardial signal was low-pass filtered by a first order Butterworth filter (< 1 Hz) and connected through linear interpolation. The final baseline was obtained after subtracting the mean and additional low-pass filtering with an identical filter. The epicardial signal was corrected for baseline wander by subtraction of the baseline. An error margin around the baseline was defined as the standard error of the mean (SEM) of the derivative of the original epicardial signal (Fig. 6). The algorithm is described in detail in the Appendix (section A1).

Figure 6

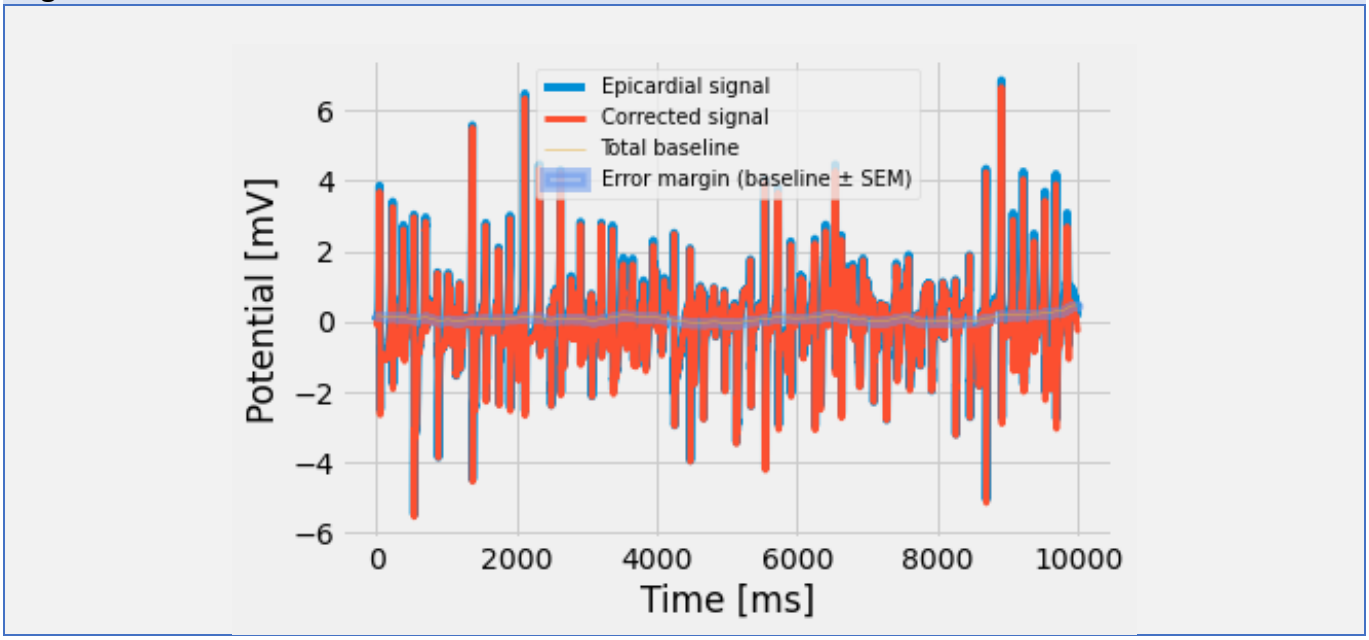

Representative example of baseline determination and correction for baseline wander. The corrected epicardial signal (red) is the difference between epicardial signal and baseline. SEM = standard error of the mean

3.2.3. Calculation of EA

The EA was determined for all primary LATs, excluding LATs occurring in exclusion windows. The limits of integration correspond with the EGM start- and endpoint, i.e. intersections between the corrected signal and the baseline ± SEM. Naturally, multiple intersections occur in the course of an EGM, especially during fractionation. Therefore the R- and S-peak were determined using a fixed window of 80 ms around the current LAT. The R-peak and S-peak were respectively defined as the first maximum of the signal and the last minimum of the signal within this window (Fig. 7). The limits of integration were the intersections between epicardial signal and baseline preceding the R-peak and following the S-peak in the same window (Fig. 7). If intersections occurred in exclusion windows or no intersections were found, nearest values were used instead. After obtaining the limits of integration, the EA was calculated as the sum of the trapezoids that fill up the area between the absolute epicardial signal and baseline ± SEM (Fig. 7). In an additional analysis, the net EA was determined by subtracting the area below baseline from the area above baseline.

Figure 7

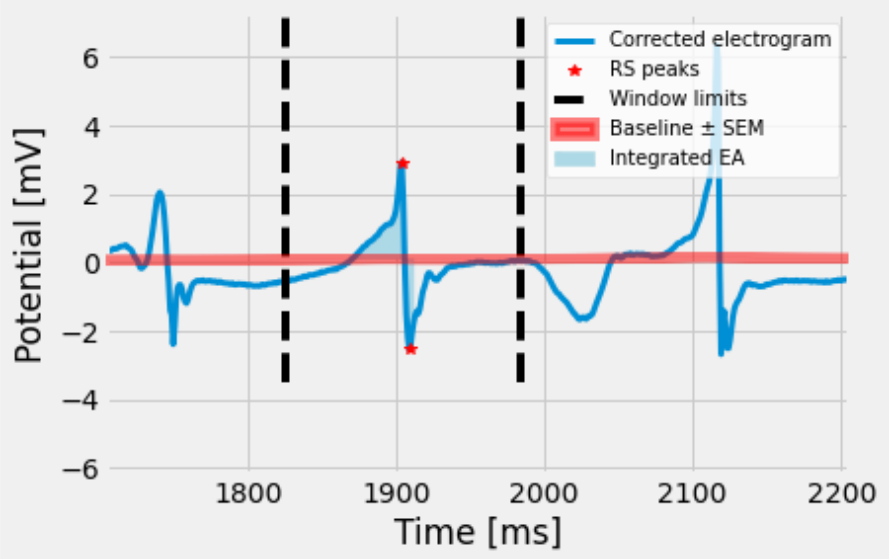

Representative example of the area of a unipolar electrogram. Note that in this example the nearest value of the EGM end point is used because the S-peak is followed by a far-field ventricular potential . SEM = standard error of the mean.

3.2.4. Primary outcomes

The EA was determined per electrode per EGM for recordings of the atrial regions RA, BB, LA and PV. The obtained values were used to determine spatiotemporal differences in EA across between rhythms (AF vs. SR), across atrial regions, and between groups (MVD with AF vs. MVD no AF). The following outcomes were determined to construct individual EA fingerprints:

$$\text{Mean EA: } \mu_{EA} = \frac{\sum EA\ of\ primary\ LATs}{N_{primary\ LATs}} \quad (5)$$

$$\text{Variance of EA: } \sigma_{EA}^2 = \frac{1}{N}\sum_{i=0}^{n-1}(x_i - \mu)^2 \quad (6)$$

$$\text{Total EA: } Tot_{EA} = \sum EA\ of\ primary\ LATs \text{ in 5 s} \quad (7)$$

Where x_i in(5) denotes a sample EA from a primary LAT and N in (5) and (6) denotes the number of primary LATs in a recording. For the total EA, AF recordings were split into two. This ensures an equal comparison between SR and AF, as SR recordings last five seconds by default while AF recordings last ten seconds.

3.2.5. Statistics

All data were tested for normality. Normally distributed data are expressed as mean ± SD and analyzed with an independent sample t-test. Skewed data are expressed as median (IQR) and analyzed with a Mann-Whitney U test. Categorical data are expressed as numbers and percentages and analyzed with a Chi-squared test or Fisher's exact test.

4. Results

4.1. Study population

Clinical characteristics of the study population, including 19 patients without ('no AF group') and 23 with AF ('AF group') are described in detail and compared in Table 1. These groups differed in BMI [no AF: 24.9 (5.25) vs. AF: 28.0 (5.85) kg/m^2, p = 0.03], in the presence of coronary artery disease [no AF: 3 (16%) vs. AF: 0, p = 0.03] and in the use of class V antiarrhythmic drugs [no AF: 1 (5%) vs. AF: 8 (35%), p = 0.01]. The

grade of mitral insufficiency and stenosis did not differ between groups, but the majority of patients suffered severe insufficiency [no AF: 11 (58%) vs. AF: 11 (48%), p = 0.55]. LA dilatation was reported in the majority of patients, but often the diameter was not documented and therefore dilatation > 45 mm might be underestimated [no AF: 9 (47%) vs. AF: 8 (42%)]. Left ventricle dysfunction was present in 3 patients without AF (16%) and in 8 patients with AF (35%). Finally, in the AF group, 16 patients were diagnosed with paroxysmal AF (69%) and 7 patients with persistent AF (30.5%). In the no AF group, one patient presented in paroxysmal AF on the operation table.

Table 1. Patient characteristics (N = 42)

	No AF	AF	p-value
Demographic characteristics			
Patients	19 (45)	23 (55)	–
Female sex	5 (26)	13 (57)	0.07
Age (years)	64.2 ± 14.1	70.1 ± 8.8	0.16
Cardiovascular risk factors			
BMI (kg/m^2)	24.9 (5.25)	28.0 (5.85)	0.03
Obese (≥ 30)	2 (11)	6 (26)	0.19
Hypertension	7 (37)	9 (39)	1.00
Dyslipidaemia	3 (16)	1 (4)	0.20
Diabetes mellitus	0	2 (9)	0.11
Coronary artery disease	3 (16)	0	0.03
Left sided cardiac characteristics			
Left atrial dilatation > 45 mm	9 (47)	8 (35)	0.53
Left ventricular dysfunction	3 (16)	8 (35)	0.16
Mitral stenosis			
No	18 (95)	19 (83)	0.36
Severe	1 (5)	4 (17)	0.36
Mitral insufficiency severity			
Mild	2 (11)	3 (13)	0.80
Moderate	3 (16)	2 (9)	0.48
Moderate-to-severe	2 (11)	4 (17)	0.52
Severe	11 (58)	11 (48)	0.55
Antiarrhythmic agents			
Class I	0	0	–
Class II	8 (42)	12 (52)	0.55
Class III	0	3 (13)	0.05
Class IV	1 (5)	1 (4)	0.89
Class V (Digoxin)	1 (5)	8 (35)	0.01

Values are presented as N (%), mean ± SD or as median (IQR).
BMI = body mass index

4.2. Data characteristics

As demonstrated in Table 2, a total of 3104460 EAs were analyzed in 832 recordings (SR: 428 recordings of 5 s, AF: 404 recordings of 10 s). There were more U-EGMs in AF compared with SR [SR: 0.37 (0.20), AF: 3.09 (2.34) * 10^5, $p < 0.01$]. The median EA of all primary LATs recorded from the entire epicardial surface was also higher in AF [SR: 54.97 (42.87), AF: 57.03 (51.02), $p < 0.01$]. There was no difference in the number of U-EGMs between the AF and no AF group [no AF: 1.13 (1.52), AF: 1.41 (3.29) , $p = 0.25$]. EA is a combination of U-EGM duration and peak-to-peak amplitude, which are observably different in AF compared with SR across all atrial regions in both the AF and no AF group.

Table 2. Data characteristics

	MVD without AF (n = 23)			MVD with AF (n = 19)		
	SR	AF	p-value	SR	AF	p-value
Right atrium						
No. of recordings	74	76	–	86	86	–
Amplitude[1] (mV)	5.42 (4.15)	3.02 (2.55)	< 0.01	5.52 (4.79)	3.06 (2.89)	< 0.01
Duration[2] (ms)	77 (49)	89 (51)	< 0.01	80 (52)	90 (51)	< 0.01
EA (mC)	55.41 (40.61)	60.24 (53.73)	< 0.01	54.97 (42.87)	57.02 (51.02)	< 0.01
Bachmann's Bundle						
No. of recordings	27	25	–	35	35	–
Amplitude[1] (mV)	6.46 (6.27)	2.46 (2.37)	< 0.01	3.69 (4.13)	1.85 (1.63)	< 0.01
Duration[2] (ms)	74 (49)	99 (50)	< 0.01	83 (43)	99 (47)	< 0.01
EA (mC)	64.84 (46.02)	60.78 (57.54)	< 0.01	42.83 (42.76)	44.19 (42.37)	< 0.01
Left atrium						
No. of recordings	40	26	–	55	54	–
Amplitude[1] (mV)	5.12 (6.00)	3.17 (3.37)	< 0.01	4.68 (4.75)	2.49 (2.78)	< 0.01
Duration[2] (ms)	82 (41)	88 (48)	< 0.01	83 (43)	88 (50)	< 0.01
EA (mC)	53.58 (52.73)	57.26 (51.77)	< 0.01	44.99 (41.19)	43.44 (40.03)	< 0.01
Pulmonary vein region						
No. of recordings	46	43	–	65	59	–
Amplitude[1] (mV)	4.89 (5.85)	2.57 (2.16)	< 0.01	3.46 (4.85)	1.88 (1.79)	< 0.01
Duration[2] (ms)	74 (42)	91 (52)	< 0.01	82 (39)	95 (52)	< 0.01
EA (mC)	53.97 (51.77)	57.13 (55.24)	< 0.01	44.49 (42.69)	40.64 (42.25)	< 0.01

Values are presented as numbers or as median (IQR)

[1] Peak-to-peak amplitude of RS-ratio as determined by algorithm.

[2] Duration of unipolar electrogram as determined by algorithm.

4.3. Individual charge fingerprints

Two representative examples of color-coded spatiotemporal distributions of EA in SR and AF for a patient with (upper panel) and a patient without AF (lower panel) are illustrated in Figure 8. The patient in the AF group suffered from persistent AF and also presented in AF during surgery. Both patients exhibit visible differences in spatial distribution of EA between SR and AF, as well as between regions. The variance and spatiotemporal total EA of the patient with persistent AF are shown for the superior RA during SR and AF in Figures 9-10. There is an evident difference in magnitude and spatial distribution of variance between SR and AF. In SR, electrodes tend to have a smaller variance compared with AF, as the EA of any primary LAT corresponds closely with the mean EA. A similar observation is made for the spatiotemporal total EA (Fig.10, note difference in axes), which is larger in AF compared with SR and differently distributed.

Figure 8

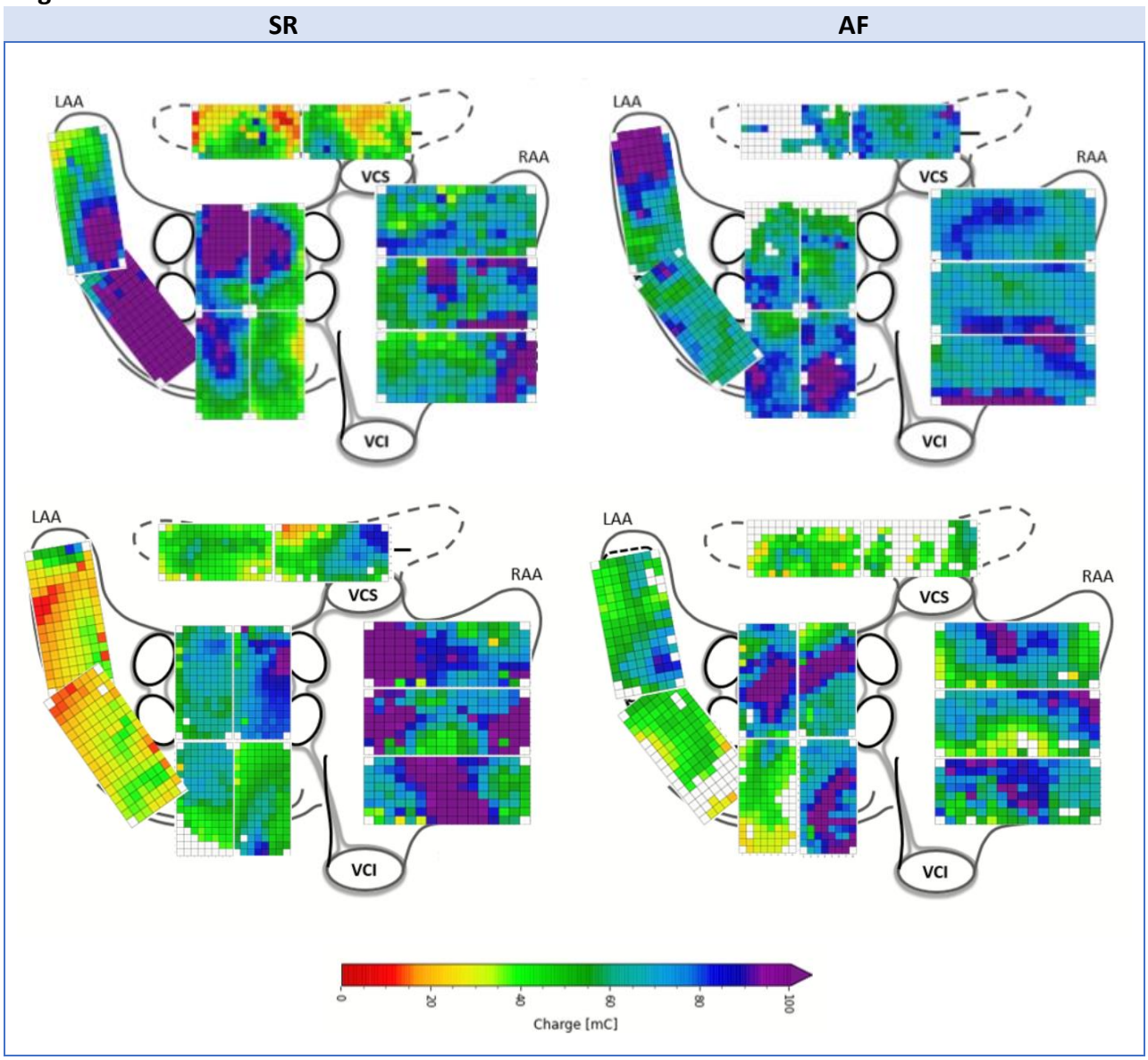

Representative examples of unipolar epicardial EA maps during SR (left) and AF (right) in a patient without AF (upper pannel) and in a patient with AF (lower panel).

Figure 9

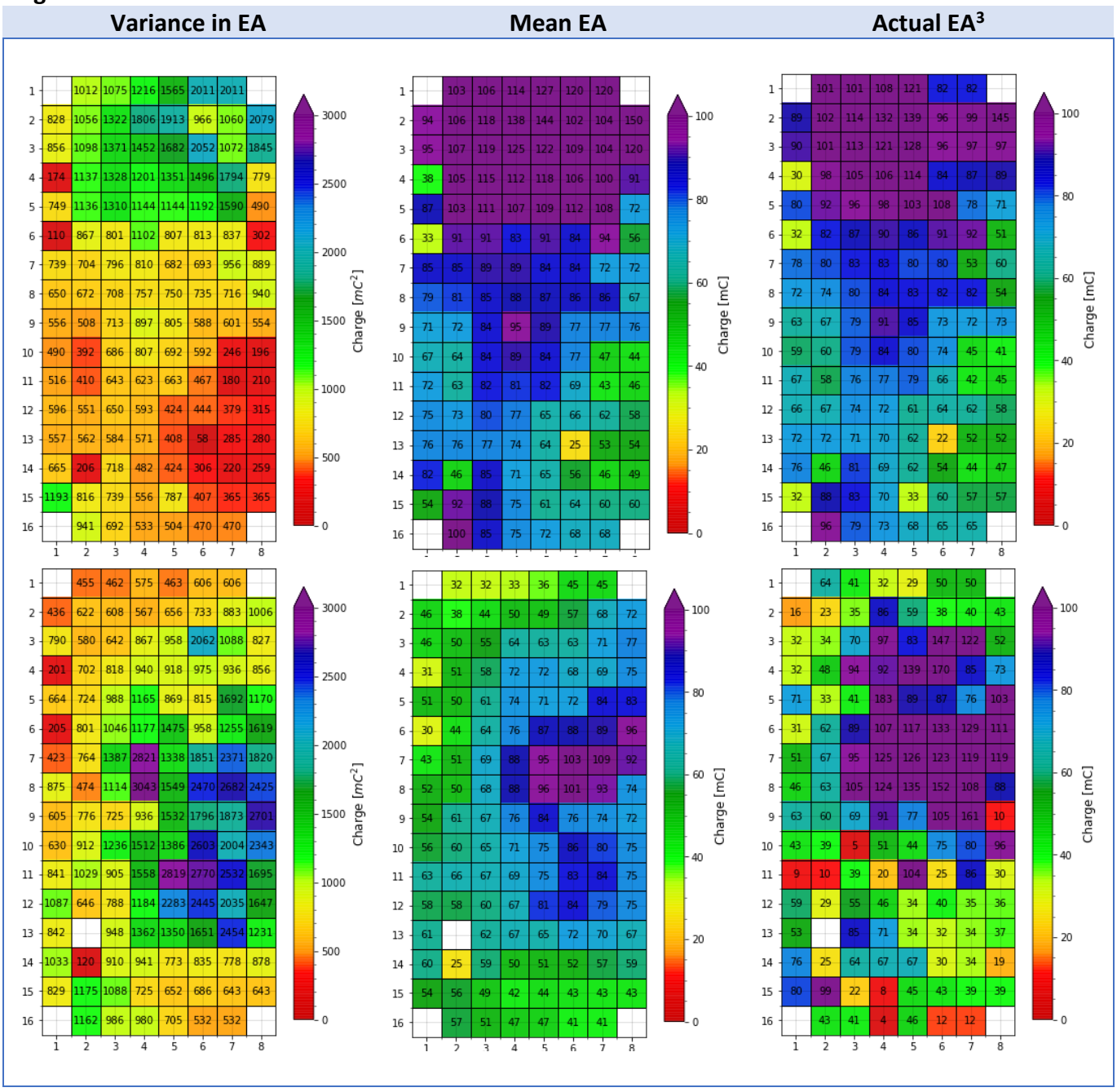

Representative example of unipolar epicardial EA variance during SR (upper panel) and during AF (lower panel) recorded from the right atrium in a patient with persistent AF.

[3] The EA determined for a random primary LAT in the recording.

Figure 10

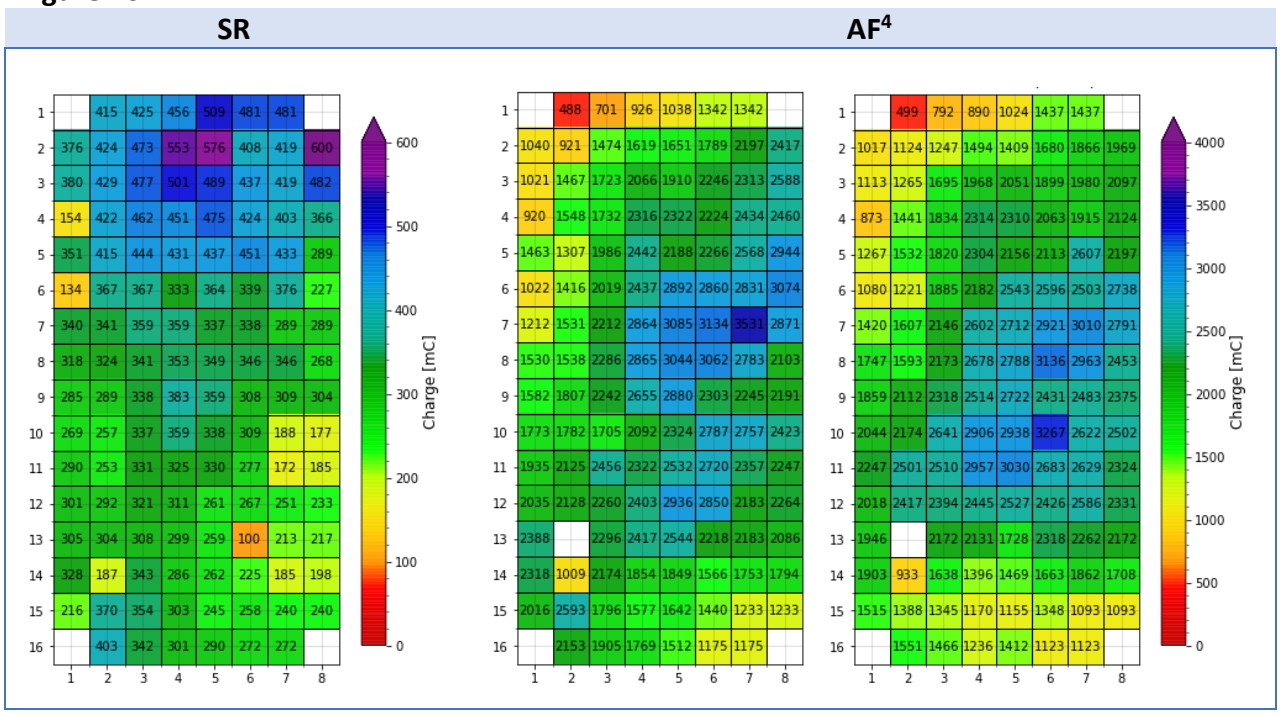

Representative example of total spatiotemporal EA during SR (first column) and during AF (second column). The magnitude on the axes between SR and AF are different.

[4] AF recordings last 10 s by default, and are therefore cut into two parts of 5 s, hence two total EA maps.

4.4. Regional differences in unipolar EA

As presented in Table 3, regional differences apply when comparing EA in SR with EA in AF. In the RA, the median EA is larger in AF [SR: 55.19 (41.74) vs. AF: 58.79 (53.16), $p < 0.01$], but in the atrial regions BB, LA and PV the median EA is smaller in AF. The biggest difference in median EA between SR and AF is found in the PV region [SR: 49.18 (42.12) vs. AF: 46.18 (47.85), $p < 0.01$]. Histograms of EA distributions across atrial regions for SR and AF recordings in both groups are available in Figure 11.

Table 3. Regional differences in EA

	SR	AF	p-value
RA	55.19 (41.73)	58.79 (53.16)	< 0.01
BB	51.89 (47.85)	51.04 (49.52)	0.04
LA	48.74 (45.80)	47.47 (44.73)	< 0.01
PV	49.18 (42.12)	46.18 (47.85)	< 0.01

Values of EA are expressed as median (IQR)

4.5. Correlation between EA and arrhythmogenic substrate

A comparison of EA in SR and in AF between groups across atrial regions is provided in Figure 11. Without a history of AF, the median EA is larger in induced AF across all regions compared with SR [RA: 60.24 (53.73) vs. 55.41 (40.61), BB: 60.78 (57.54) vs. 64.84 (46.02), LA: 57.26 (51.77) vs. 53.58 (52.73), PV: 57.13 (55.24) vs. 53.97 (51.77), $p < 0.01$ for all regions]. With a history of AF, the median EA is only larger in AF in RA [AF: 57.02 (51.02) vs. SR: 54.97 (42.87), $p < 0.01$] and across BB [AF: 44.19 (42.37) vs. SR: 42.83 (42.76), $p < 0.01$]. The EA is smaller during AF in LA [AF: 43.44 (40.03) vs. SR: 44.99 (41.19), $p < 0.01$] and in the PV region [AF: 40.64 (42.25) vs. SR: 44.49 (42.69), $p < 0.01$] compared with SR. Comparing the no AF group with the AF group reveals that, for both rhythms and across all regions, median EA is significantly smaller in the AF group. The largest differences between groups are found across BB, followed by LA-PV. Fluctuations

in EA across atrial regions and between rhythms are evidently larger in the AF group. In the no AF group, the median EA varies in a smaller range in both SR and AF, the latter displaying the smallest variability.

Figure 11

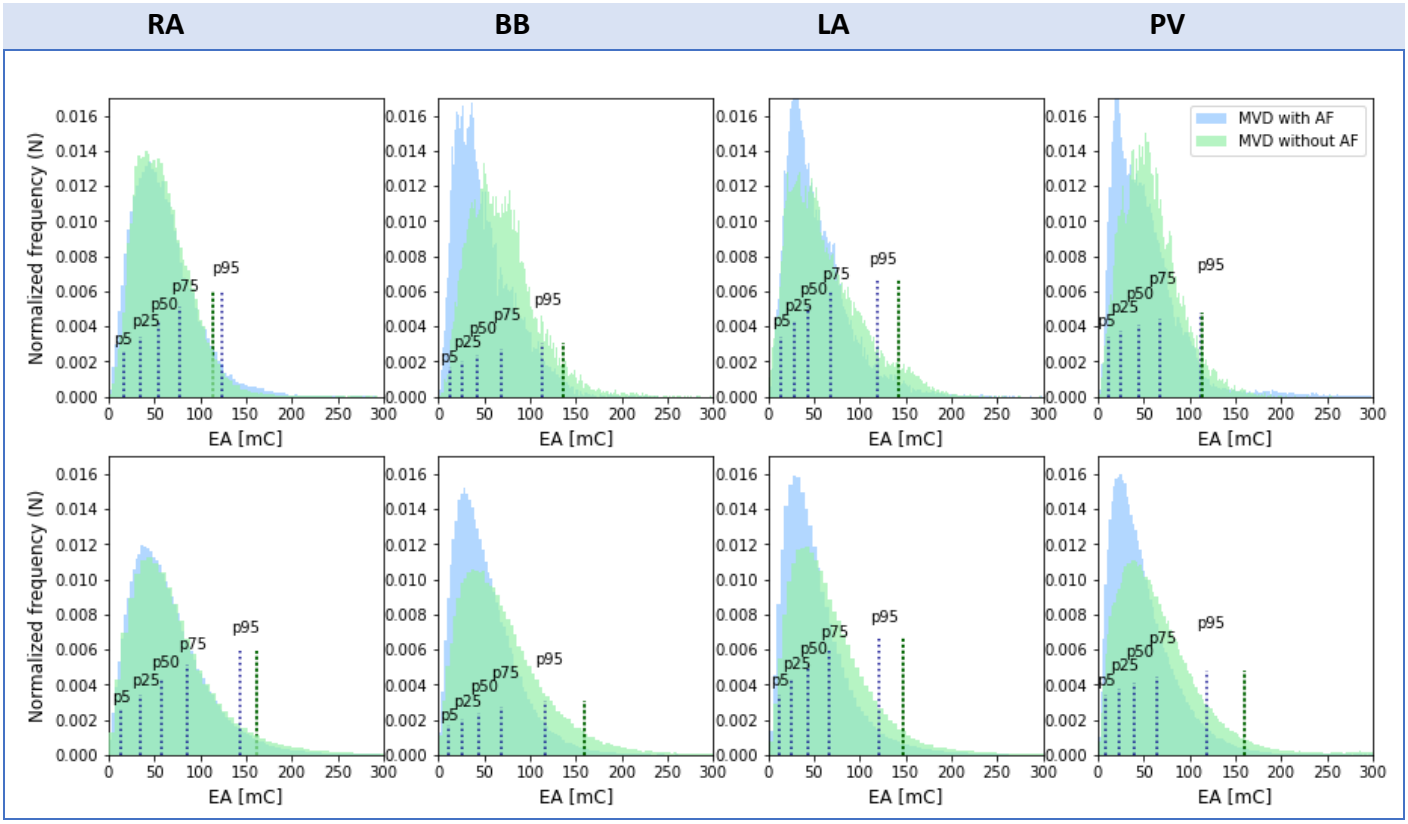

Normalized histograms of EA distributions across the atrial regions in SR (upper panel) and AF (lower panel) for the no AF (green) and AF group (blue). Each histogram displays the number of data points (y-axis) for each value of EA (x-axis). A vertical peak indicates a high frequency of data points, while a wide morphology indicates higher values of EA. The dashed vertical lines correspond with the 5th, 25th, 50th, 75th and 95th percentile.

4.6. Correlation between EA and signal morphology

The relation between EA and peak-to-peak amplitude is illustrated in Figure 12, and the distribution of net EA across the atrial regions is portrayed in Figure 13. As illustrated in Figure 12, there is no clear correlation between EA and amplitude, though in both groups the correlation coefficient is stronger in SR [no AF: r = 0.64, p = 0.00 vs. AF: r = 0.63, p = 0.00] compared with AF [no AF: r = 0.54, p = 0.00 vs. AF: r = 0.51, p = 0.00]. A representative example of U-EGM morphologies corresponding with EA sizes is available in Figure A4 in the Appendix. As illustrated in Figure 13, the net EA is different between SR and AF across all atrial regions. Similarities and differences between the AF and no AF group can be observed. Note that outliers are not shown here, the boxplot with outliers is available in the Appendix (Section A2, Fig. A5).

Figure 12

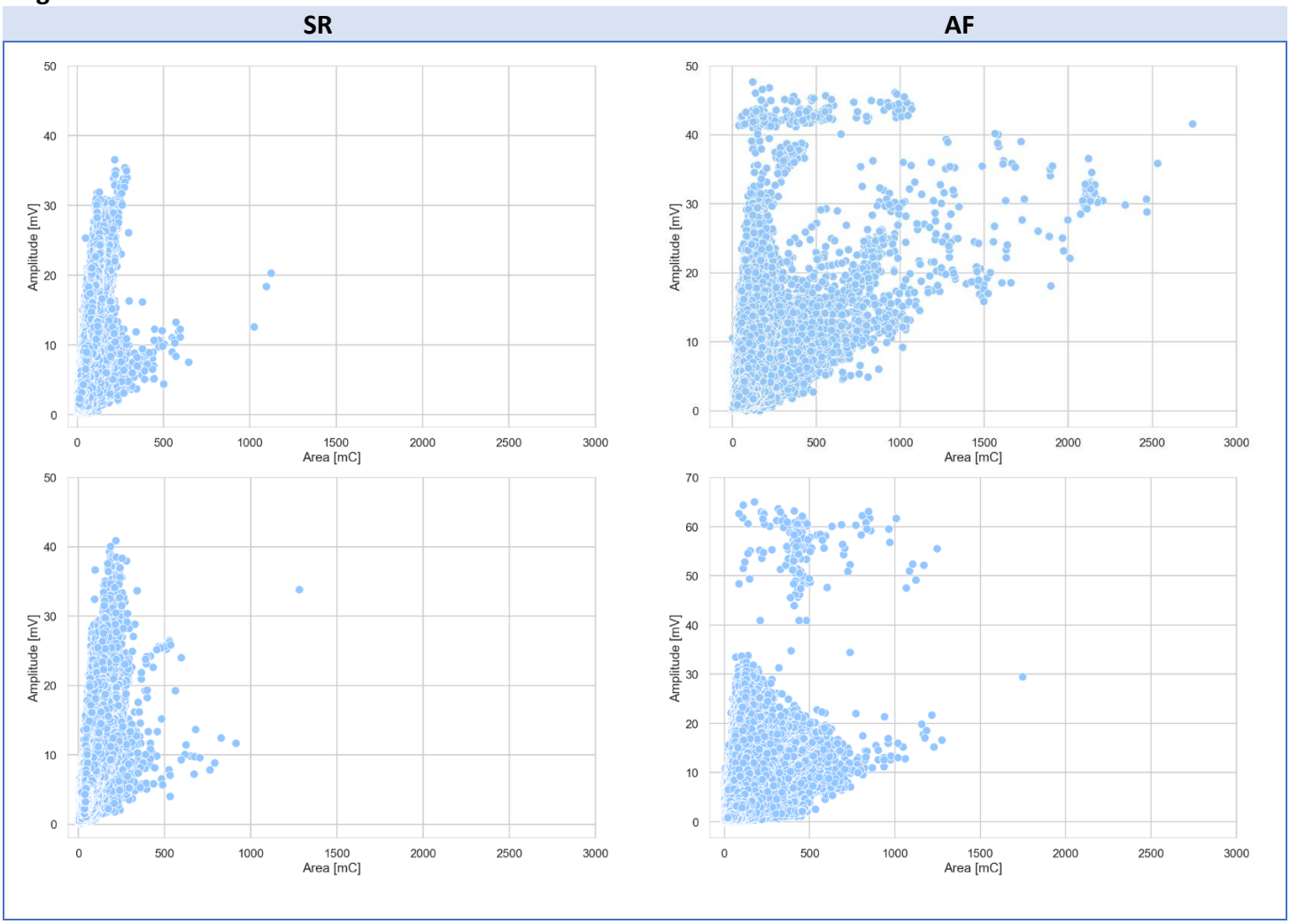

Scatterplots of the correlation between EA and U-EM amplitude for patients without AF (upper row) and patients with AF (bottom row), during SR (left) and AF (right).

Figure 13

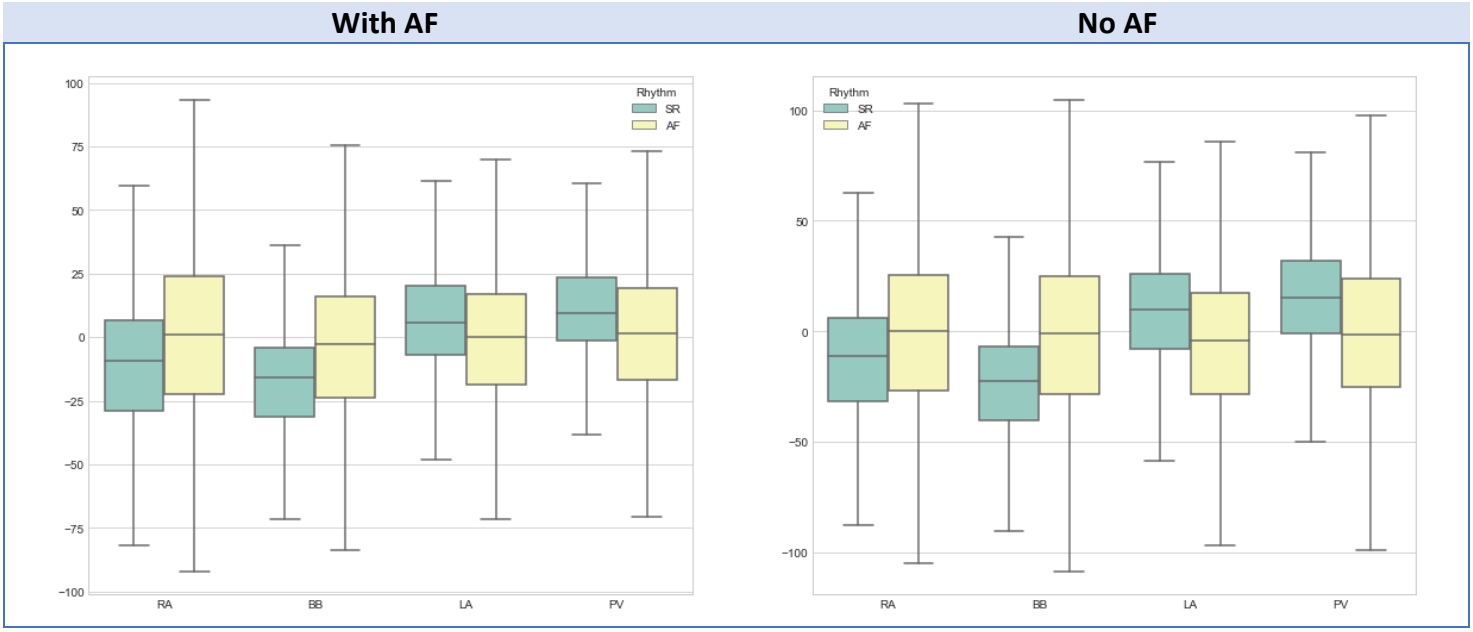

Boxplots without outliers of net EA across all atrial regions in the AF (left) and no AF group (right).

5. Discussion

In the present study, we determined high-resolution unipolar EAs in patients with MVD and demonstrated variations in spatial distributions of EA between SR and AF, across atrial regions and between patients with or without a history of AF. EA is the resultant of U-EGM amplitude, duration and morphology, specifically the RS-ratio, and contains valuable information about individual electropathology. In AF and even in SR, patients with a history of AF have smaller EAs across all atrial regions. Predilection sites where differences in EA between rhythms and groups were most prominent were found at BB and the PV region.

4.1 Unipolar EA mapping in signal fingerprinting

Electric charge in atrial tissue can be approximated from the spatial distribution of U-EGM areas, hereby referred to as EA mapping. The unipolar electrode configuration is increasingly used in substrate mapping as it provides more accurate information on the arrhythmogenic substrate compared with the bipolar electrode configuration. (8, 11-15) The biphasic morphology of the U-EGM implies the area consists of a part above baseline (positive) and a part below baseline (negative). (17) The absolute EA is the sum of the areas, while the net EA is the difference between the two. Variation in amplitude and RS-ratio across atrial regions during SR and AF, will influence both the absolute and net EA. Asynchronous activity reduces the amplitude, while a loss of conductive properties prolongs the U-EGM duration. (6, 8) Alterations in RS-ratio change the respective sizes of the positive and negative area. All of the prior will thus influence the EA, as shown in the present study. This study is the first to consider the area of U-EGMs as a feature in signal fingerprinting. Fingerprinting based on voltage and morphology by Starreveld et al., van Schie et al. and Ye. et al. have shown extensive inter-individual and regional differences (5, 7, 8). The present study shows that the magnitude and direction of change in EA is determined by an interplay of amplitude, duration and morphology, specifically the RS-ratio. During AF, a single amplitude value produces a larger variation of EAs compared with SR (Fig.12) and net EA varies between SR and AF according to RS-ratio (Fig.13). This finding underlines the need to approach or voltage with caution (6-8, 11, 17, 46). A benefit of EA is that it is a morphological evaluation as well as proxy for electric charge. Though AF is associated with conduction disorders, charge levels during AF remain a subject of research. In 2013, Grey et al. modelled myocardial transmembrane currents during episodes of ventricular fibrillation (VF), an arrhythmia similar to AF that affects the ventricles (44). It was found that during VF a new equilibrium in ionic currents was established and charge density across the cell membrane increased. Although we did not determine the charge density in the present study, we did encounter reductions in median EA between rhythms and between groups with or without a history of AF. Recently, Mendonca Costa et al. reported a linear correlation (r^2 = 0.92) between the amplitude-normalized EA of a bipolar electrogram and the level of local conduction delay in tachyarrhythmias (16). Conduction delay resulted in a larger EA through broadening of U-EGM morphology, similar to our findings in the present thesis. However, the bipolar EGM is a function of the temporal offset between the electrode pair, and as such inherently dependent on the propagation speed of a wavefront in the medium. (17) For that reason, the present study is considered to have a more suitable methodology to investigate EA in tachyarrhythmias such as AF.

4.2 Interrelationship between EA and arrhythmogenicity

Commonly associated with AF are uncoordinated electrical activity, a loss of conductive properties and depolarization of multiple independent areas (10, 21-24, 39, 40). Albeit slight, we found the median EA to be larger in AF compared with SR [SR: 54.97 (42.87), AF: 57.03 (51.02) mC, $p < 0.01$]. Considering the large number of EAs analyzed, this minor difference may lack practical meaning. It should also be noted that the median no. of EAs was larger in AF as a result from tachycardia [SR: 0.37 (0.20), AF: 3.09 (2.34) * 10^5, $p < 0.01$]. Nonetheless, in the majority of patients we also found the mean EA, EA variance and spatiotemporal

total EA to be larger in AF compared with SR. Clear differences in spatial distributions of mean EA between SR and AF can be observed in the fingerprints (Fig. 8). Aside from regional and inter-patient differences, the alternating color map indicates larger EAs during AF in certain areas. A number of electrodes also remain 'empty' indicating diseased tissue. All of the prior underlines the prominence of electrical heterogeneity and conductive disorders in AF. Enhanced heterogeneity is also illustrated by a weak correlation between the mean EA and the actual EA of a random primary LAT, resulting in larger EA variance in AF (Fig. 9). We also found a larger spatiotemporal total EA in AF compared with SR (Fig. 10). However, this may be partly attributable to the higher number of U-EGMs per second in AF resulting from tachycardia.

Findings of the present study have shown that the larger EA in AF is caused by broader U-EGM morphology (Table 2). While the amplitude is significantly reduced in AF, the duration is prolonged conform findings by Mendonca Costa et al (16). Hence, low-amplitudes should be approached with caution as shown in voltage fingerprinting. (6) Prolonged U-EGM duration in AF may be explained by fractionation and/or conduction disorders. The majority of patients were paced to induce AF on the operation table. Induced AF through pacing may result in a more synchronous activation of the myocardium than in pathological AF and thus a larger amplitude. Finally, if we incorporate the relation between charge and EA, cardiac pacing may enlarge the EA by adding energy to the tissue. Tachycardia is known to reduce the effective refractory period, resulting in shorter action potential durations (47-49). Given that conduction is the displacement of charged particles, this new balance between inward and outward currents may account for the slower conduction and prolonged U-EGM duration observed during AF.

4.3 Regional differences in EA

Different atrial regions have different conductive properties. The present study also demonstrates evident regional differences in EA. Firstly, median EA decreases from the RA to the LA-PV region via BB (Table 3), with slight increases in the PV region in SR and in the LA region in AF. A decrease in EA over this trajectory is consistent with the direction of atrial conduction, as activation starts in the RA and then proceeds to the LA-PV-region over the specialized, fast-conducting tissue of BB. (50) However, local sites of large EA are visible across all atrial regions (Fig. 8). As described by Sim et al., the transmembrane current is driven by a potential gradient from active to resting tissue. Given that charge is the time-integral of current, and EA is considered a proxy of charge, it is plausible for regions to display local sites of large EA (17).

The largest EA during AF and SR is found across the RA (Table 3). The RA contains the SAN, a cluster of cardiac pacemaker cells to generate electrical activity (51). Compared with the working myocardium, the resting membrane potential of SAN cells is relatively low (–60 mV vs. –90 mV) (52). Depolarization of the SAN activates a wavefront that is rapidly conducted through low resistance gap junctions (52). Activation sites are characterized by monophasic S-waves and fast propagation results in high-amplitudes with a variation of S-waves and biphasic RS-waves (6). Hence, during SR the net EA is negative (Fig.13) but the absolute EA is large given a constant U-EGM duration in SR (Table 2). EA only appears to increase from SR to AF across RA, which may be explained by the relatively larger increase in U-EGM duration compared with amplitude reduction here. However, results could have been influenced by the fact that the majority of SR and AF recordings in both groups were of the RA [no AF: 150 (42%) vs. AF: 172 (36%)]. As a result, the increase in median EA during AF compared with SR for the myocardium as a whole may also rely mainly on the increase observed in the RA. All other exhibit a decrease in median EA in AF compared with SR. BB is the interatrial pathway comprising parallel aligned cardiac muscle strands. Specialized conductive tissue and anisotropic fiber orientation ensures fast-conduction and hence, in SR the largest amplitudes are measured across BB (40, 50). Median EA across BB is slightly decreased in AF compared with SR (Table 3). Differences are larger when we compare EA SR with AF within the respective groups of AF history (Table 2). Here, we also found that the decrease in median EA results from a larger decrease in amplitude relative to the increase in U-EGM duration. An explanation is that BB is a predilection site for conduction disorders in

AF. On the contrary to absolute EA, net EA across BB increases in AF compared with SR, conform a shift from S-wave predominance towards R(-S)-wave predominance. Coincidentally, research has shown that BB displays the largest differences in S-wave amplitudes. (6) The LA-PV regions both show larger decreases in median EA in AF compared with SR (Table 3). In addition, the net EA is also reduced during AF across these two regions, resulting from combination of R-wave predominance and low amplitudes in SR, which are even further reduced during AF (Fig.13, Table 2). In MVD patients, the LA-PV region comprises the diseased area. In the majority of patients the LA was enlarged, though this number may have been higher since the diameter was not always documented [no AF: 9 (47%) vs. AF: 8 (42%)]. Considering the prior, the LA-PV region is also prone to conduction disorders during AF (40, 50). We also find lower amplitudes here during SR (Table 2). From an anatomical perspective, the LA has a thicker atrial wall compared with the RA and is additionally covered by a layer of fibro-fatty tissue. Hence, signals may be attenuated here (53-56). Finally, the PV region also plays a prominent role in generating AF triggers and is therefore a frequent ablation site (34, 36, 42, 56). This may explain why during SR, median EA is larger across the PV region compared with the LA region (Table 3). The increase is also observed in the net EA (Fig.14), possibly indicating heightened R-wave predominance and/or increased R-wave amplitudes (6).

4.4 Structural remodeling and electropathology

Patients undergoing MVD surgery are assumed to have advanced structural remodeled atria even without a history of AF, due to the interplay of pressure and/or volume overload (8, 57, 58). However, a history of AF also introduces advanced electrical remodeling and contributes to the arrhythmogenic substrate (47). We found median EAs to be lower in patients with AF versus patients without a history of AF (Table 2). This finding is valid across all atrial regions. Research has shown that during SR, patients with AF tend to have a loss of amplitude, especially a loss of S-wave amplitude (6, 8, 11, 17). This is consistent with findings of the present study, where during SR patients with a history of AF show lower amplitudes across all atrial regions and the net EA is relatively more positive across regions with S-wave predominance (RA and BB) compared with patients without a history of AF (Table 2 & Fig. 14). Naturally, the absolute EA is also lower. The largest differences in EA between the AF and no AF group are observed at BB and LA-PV (Table 2). As mentioned prior, BB and LA-PV are, respectively, a predilection site for conduction block and a target in AF ablation. On the contrary, in the RA, where the EA difference between groups is relatively minor, electrical activity remains prominent due to the SAN. The with AF group also displays larger fluctuations in median EA throughout the atrial regions compared with the no AF group. Findings suggest that EA is influenced by the degree of electropathology in the atria. An explanation is electrical remodeling and in particular, ion channel remodeling as described prior by Voigt et al., Colman et al. and Nattel et al. (48, 59, 60). Ionic currents are altered, among which a reduction in sodium current density, a reduction in transient outward potassium current amplitude and an increase in inward rectifier potassium current amplitude. The effect is a higher peak inward current versus the peak outward current and an increased charge density over the cell membrane conform findings by Gray et al. during VF (44) . Thus, more charge intracellular relative to extracellular compared with normal cardiac electrophysiology. Furthermore, the presence of conduction block and fibrosis in electrically remodeled atria leads to a loss of conduction, hence a loss of charge in these sites. Altogether this suggest that EA, serving as a proxy for electric charge, is thus reduced by electrical remodeling. The direct evidence for this is illustrated by the difference in median EA found between the groups in Table 2 and in Figure 11.

Since AF is a multi-layered problem and we only mapped the epicardium (or outer layer), the measured signal might be more of a net effect rather than a pure epicardial signal (28). That it unless we assume that the epicardium is the only layer that propagates wavefronts. However, recent studies which also mapped the endocardium have shown the opposite to be true (28, 37, 41, 61). Between endo- and epicardium is also a middle layer that remains untouched thus far in research. The measured epicardial signal is therefore a resultant of all underlying activity as measured by the electrodes. Individual U-EGMs and their areas are

then the net result of interference between multiple deflections, which are added or subtracted according to their timing cycles. In theory, a measured EA of zero might not imply an actual epicardial EA of zero, but merely a net EA of zero due to U-EGMs of different layers cancelling each other out. Be that as it may, it's currently not possible to measure the layers between epi- and endocardium. Continuing, the same problem applies when using other features such as RS-ratio, or peak-to-peak amplitude. If multiple layers produce U-EGMs with different timing cycles, the net U-EGM amplitude is attenuated or intensified accordingly. In fact, we've seen that the ability of amplitude to serve as a proxy for EA is diminished in AF. The spatial distribution of EA can reflect on local bulks of charge that may originate from within the myocardium, since the amount of myocardium is not altered during the mapping procedure. This provides us with a whole new insight into individual electropathology compared with conventional substrate mapping.

4.5 Study limitations

The relation between EA and charge is based on a mathematically derived model. However, calculations in Python employ the trapezoidal rule and mainly use the absolute signal, which differs from equations (1)-(3). In addition, we assume a uniform resistance throughout the atria. However, in reality there is spatial variation in resistance and hence, conductivity, due to tissue inhomogeneity and electrical anisotropy (62, 63). While RA has a thin muscular wall, LA has a thicker wall and LA and BB are covered by a layer of fibro-fatty tissue (54, 64). However, the objective of the present study was to evaluate EA as a fingerprinting feature, and to provide a rough estimate of charge distribution in the atria. A second limitation is the method of annotation using custom software during preprocessing. When using this method, long-duration potentials are cleared as well as electrodes with < 20 deflections annotated. In addition, the annotation process is prone to subjectivity and human error. This could introduce 'annotation bias' in the results. Notwithstanding, this method was established on the department based on empirical research, and has been in use for nearly a decade with successful result. A number of annotated files were reviewed by independent researchers at the department to ensure sufficient quality of annotation. A final limitation is that the present study was conducted only in MVD patients. Per contra, considering the prominent role of MVD in AF pathophysiology it was deemed the most suitable research group to start. MVD exists as regurgitation or stenosis and results in a volume overload in the LA, which increases atrial pressure. Over time, dilatation of the LA is induced along with structural damage and cardiac remodeling. The latter is a direct cause of tachyarrhythmias such as AF, and for this reason MVD often coexists with (severe) AF.

4.6 Clinical implications

When we compare EA to other U-EGM parameters, for example the unipolar peak-to-peak amplitude, its added value becomes evident. As mentioned prior, amplitude is often used to describe the arrhythmogenic substrate. Low-voltage areas are even regarded as targets during AF ablation (8, 11, 17, 56). Nonetheless, low-voltage areas should be approached with caution as they are also found during SR and in patients without a history of AF, lacking evident predilection sites (8). We found that the correlation between amplitude and EA barely approximates strong at best ($r = 0.63 – 0.64$) and is moderate at worst ($r = 0.51 – 0.54$). A clear pattern is lacking when we compare U-EGM amplitude with its area (Fig. 12). In SR, values of amplitude and EA tend to follow a pattern. Low amplitudes coincide with small EAs and slight increases in amplitude results in drastically larger EAs. This suggests that in SR, U-EGM duration is relatively constant across the atrial regions as also shown in Table 2 [no AF: range 74-82 vs. AF: range 80-83 ms]. Moreover, during SR regions exhibit typical RS-ratios as reflected by the net EA (Fig.13), which also contributes to a fairly uniform amplitude-EA pattern. However, during AF the amplitude-EA pattern becomes dispersed and prone to outliers. The majority of data points exhibit a lower amplitude, although some high amplitudes are observable (Fig.12). A given amplitude also produces a large range of EA values (Fig.13). Hence, U-EGM duration is more variable in AF, as also illustrated in Table 2 [no AF: range 88-99 vs AF: range 88-99 ms]. In addition, the typical pattern of RS-ratios in the atria is affected during AF, resulting in deviations in net EA

during AF compared with SR (Fig. 13). All of the prior suggests that amplitude may be a proxy for EA during SR, but not in AF. During AF, EA as a descriptor of the amplitude over time, contains additional information.

Finally, the present thesis is clinically relevant as it contributes to the design of a novel diagnostic tool that is able to detect AF at the earliest possible stage, and aids in a novel classification system based on the individual degree of electropathology. To date, diagnosis often comes too late as it is only able to catch AF as episodes become more frequent and longer-lasting. Although the current classification of paroxysmal, persistent, longstanding persistant and permanent AF take this partly into account, it is mostly based on whether or not electric cardioversion is applicable. Clinically this lacks patient-specific information and that is also why patient-tailored therapy is currently not possible for AF. Although the individual AF patient might not directly benefit from the present study, it is a step towards a brighter future. It should be noted that our algorithm is based on epicardial mapping, which is an invasive procedure only indicated when undergoing open heart surgery. However, improvements have been made towards reconstruction of epicardial signals from ECG. This would allow a widespread implementation of EA fingerprinting.

4.7 Future perspectives

Additional research is required to further develop EA as a feature in signal fingerprinting. In a next step, classification based on EA values should be tested and compared to classification by existing features, such as amplitude. The present study has shown that there is a difference between amplitude and EA, and that EA contains additional and valuable information during AF. It may also be worth further exploring the net EA, as studies have shown that RS-ratios are different across the atrial regions, and their predominance within regions becomes altered in AF. Finally, following the relation between EA and charge, approximating atrial resistance is pivotal to determine the actual charge distribution. A final fingerprint ideally comprises a combination of features, as no feature alone can fully describe the individual degree of electropathology.

6. Conclusion

High-resolution unipolar EA mapping in MVD patients demonstrated evident differences between SR and AF, across atrial regions and between patients with or without a history of AF. Despite reductions in amplitude, EA was higher in AF compared with SR, reflecting a broadening of U-EGM morphology. Though regional differences apply, EA was lower in patients with a history of AF compared with patients without a history of AF. Moreover, EA was shown to correlate moderately with peak-to-peak amplitude and to be co-dependent on RS-morphology, which underlines the additional information it contains. Considerable intra- and inter-individual variation in spatial distributions of EA demonstrates the essence of individualized fingerprints. Further studies are required to fine-tune the EA and to implement EA-based classification.

References

1. Go AS, Hylek EM, Phillips KA, Chang Y, Henault LE, Selby JV, et al. Prevalence of Diagnosed Atrial Fibrillation in AdultsNational Implications for Rhythm Management and Stroke Prevention: the AnTicoagulation and Risk Factors In Atrial Fibrillation (ATRIA) Study. Jama. 2001;285(18):2370-5.
2. Lippi G, Sanchis-Gomar F, Cervellin G. Global epidemiology of atrial fibrillation: An increasing epidemic and public health challenge. Int J Stroke. 2021;16(2):217-21.
3. Zimetbaum P. Atrial Fibrillation. Annals of Internal Medicine. 2017;166(5):ITC33-ITC48.
4. Wolf PA, Mitchell JB, Baker CS, Kannel WB, D'Agostino RB. Impact of Atrial Fibrillation on Mortality, Stroke, and Medical Costs. Archives of Internal Medicine. 1998;158(3):229-34.
5. Starreveld R, Knops P, Ramos KS, Roos-Serote MC, Bogers A, Brundel B, et al. Atrial fibrillation fingerprinting; spotting bio-electrical markers to early recognize atrial fibrillation by the use of a bottom-up approach (AFFIP): Rationale and design. Clin Cardiol. 2020;43(6):546-52.
6. van Schie MS, Starreveld R, Roos-Serote MC, Taverne Y, van Schaagen FRN, Bogers A, et al. Classification of sinus rhythm single potential morphology in patients with mitral valve disease. Europace. 2020;22(10):1509-19.
7. Ye Z, van Schie MS, de Groot NMS. Signal Fingerprinting as a Novel Diagnostic Tool to Identify Conduction Inhomogeneity. Frontiers in Physiology. 2021;12(375).
8. van Schie MS, Starreveld R, Bogers AJJC, de Groot NMS. Sinus rhythm voltage fingerprinting in patients with mitral valve disease using a high-density epicardial mapping approach. EP Europace. 2021;23(3):469-78.
9. Yaksh A, van der Does LJ, Kik C, Knops P, Oei FB, van de Woestijne PC, et al. A novel intra-operative, high-resolution atrial mapping approach. J Interv Card Electrophysiol. 2015;44(3):221-5.
10. Kik C, Mouws E, Bogers A, de Groot NMS. Intra-operative mapping of the atria: the first step towards individualization of atrial fibrillation therapy? Expert Rev Cardiovasc Ther. 2017;15(7):537-45.
11. Natasja MSdG, Martin JS, Katja Z, Nico AB, Enno TVdV, Ernst EVdW. Voltage and Activation Mapping. Circulation. 2003;108(17):2099-106.
12. de Bakker JM. Electrogram recording and analyzing techniques to optimize selection of target sites for ablation of cardiac arrhythmias. Pacing and clinical electrophysiology : PACE. 2019;42(12):1503-16.
13. Kimber S, Downar E, Masse S, Sevaptsidis E, Chen T, Mickleborough L, et al. A Comparison of Unipolar and Bipolar Electrodes During Cardiac Mapping Studies. Pacing and Clinical Electrophysiology. 1996;19(8):1196-204.
14. Konings KTS, Smeets JLRM, Penn OC, Wellens HJJ, Allessie MA. Configuration of Unipolar Atrial Electrograms During Electrically Induced Atrial Fibrillation in Humans. Circulation. 1997;95(5):1231-41.
15. van der Does LJME, Knops P, Teuwen CP, Serban C, Starreveld R, Lanters EAH, et al. Unipolar atrial electrogram morphology from an epicardial and endocardial perspective. Heart Rhythm. 2018;15(6):879-87.
16. Mendonca Costa C, Anderson GC, Meijborg VMF, O'Shea C, Shattock MJ, Kirchhof P, et al. The Amplitude-Normalized Area of a Bipolar Electrogram as a Measure of Local Conduction Delay in the Heart. Front Physiol. 2020;11:465.
17. Sim I, Bishop M, O'Neill M, Williams SE. Left atrial voltage mapping: defining and targeting the atrial fibrillation substrate. J Interv Card Electrophysiol. 2019;56(3):213-27.
18. Boron WF, Boulpaep EL. Boron & Boulpaep Concise Medical Physiology E-Book: Elsevier Health Sciences; 2020.
19. Pellman J, Sheikh F. Atrial fibrillation: mechanisms, therapeutics, and future directions. Compr Physiol. 2015;5(2):649-65.
20. German DM, Kabir MM, Dewland TA, Henrikson CA, Tereshchenko LG. Atrial Fibrillation Predictors: Importance of the Electrocardiogram. Ann Noninvasive Electrocardiol. 2016;21(1):20-9.
21. Markides V, Schilling RJ. Atrial fibrillation: classification, pathophysiology, mechanisms and drug treatment. Heart. 2003;89(8):939.
22. Wijesurendra RS, Casadei B. Mechanisms of atrial fibrillation. Heart. 2019;105(24):1860.
23. Iwasaki Y-k, Nishida K, Kato T, Nattel S. Atrial Fibrillation Pathophysiology. Circulation. 2011;124(20):2264-74.
24. Schotten U, Verheule S, Kirchhof P, Goette A. Pathophysiological Mechanisms of Atrial Fibrillation: A Translational Appraisal. Physiological Reviews. 2011;91(1):265-325.
25. Lanters EA, van Marion DM, Kik C, Steen H, Bogers AJ, Allessie MA, et al. HALT & REVERSE: Hsf1 activators lower cardiomyocyt damage; towards a novel approach to REVERSE atrial fibrillation. J Transl Med. 2015;13:347.

26. de Vos CB, Pisters R, Nieuwlaat R, Prins MH, Tieleman RG, Coelen R-JS, et al. Progression From Paroxysmal to Persistent Atrial Fibrillation: Clinical Correlates and Prognosis. Journal of the American College of Cardiology. 2010;55(8):725-31.
27. Valentin F, Lars ER, Richard WA, David SC, Harry JC, Robert LF, et al. ACC/AHA/ESC Guidelines for the Management of Patients With Atrial Fibrillation: Executive Summary A Report of the American College of Cardiology/American Heart Association Task Force on Practice Guidelines and the European Society of Cardiology Committee for Practice Guidelines and Policy Conferences (Committee to Develop Guidelines for the Management of Patients With Atrial Fibrillation) Developed in Collaboration With the North American Society of Pacing and Electrophysiology. Circulation. 2001;104(17):2118-50.
28. van Marion DM, Lanters EA, Wiersma M, Allessie MA, Brundel BB, de Groot NM. Diagnosis and Therapy of Atrial Fibrillation: The Past, The Present and The Future. J Atr Fibrillation. 2015;8(2):1216.
29. Lanters EAH, Knops P, Kik C, de Groot NMS. Atrial fibrillation: A never ending story? Clin Case Rep. 2019;7(12):2368-70.
30. Hodgkin AL, Huxley AF. A quantitative description of membrane current and its application to conduction and excitation in nerve. 1952. Bull Math Biol. 1990;52(1-2):25-71; discussion 5-23.
31. Abdi B, Hendriks RC, van der Veen A-J, de Groot NMS. A compact matrix model for atrial electrograms for tissue conductivity estimation. Computers in Biology and Medicine. 2019;107:284-91.
32. Sim I, Bishop M, O'Neill M, Williams SE. Left atrial voltage mapping: defining and targeting the atrial fibrillation substrate. Journal of Interventional Cardiac Electrophysiology. 2019;56(3):213-27.
33. Starreveld R, van der Does LJME, de Groot NMS. Anatomical hotspots of fractionated electrograms in the left and right atrium: do they exist? EP Europace. 2018;21(1):60-72.
34. Blandino A, Bianchi F, Grossi S, Biondi-Zoccai G, Conte MR, Gaido L, et al. Left Atrial Substrate Modification Targeting Low-Voltage Areas for Catheter Ablation of Atrial Fibrillation: A Systematic Review and Meta-Analysis. Pacing Clin Electrophysiol. 2017;40(2):199-212.
35. de Bakker JMT, Wittkampf FHM. The Pathophysiologic Basis of Fractionated and Complex Electrograms and the Impact of Recording Techniques on Their Detection and Interpretation. Circulation: Arrhythmia and Electrophysiology. 2010;3(2):204-13.
36. Katritsis DG, Pantos I, Efstathopoulos EP. Catheter ablation of atrial fibrillation guided by electrogram fractionation and dominant frequency analysis. Expert Rev Cardiovasc Ther. 2011;9(5):631-6.
37. Mouws E, Lanters EAH, Teuwen CP, van der Does L, Kik C, Knops P, et al. Epicardial Breakthrough Waves During Sinus Rhythm: Depiction of the Arrhythmogenic Substrate? Circ Arrhythm Electrophysiol. 2017;10(9).
38. van der Does LJME, Yaksh A, Kik C, Knops P, Lanters EAH, Teuwen CP, et al. QUest for the Arrhythmogenic Substrate of Atrial fibRillation in Patients Undergoing Cardiac Surgery (QUASAR Study): Rationale and Design. J Cardiovasc Transl Res. 2016;9(3):194-201.
39. de Groot NMS, Allessie MA. Pathophysiology of atrial fibrillation: Focal patterns of activation. Pacing and Clinical Electrophysiology. 2019;42(10):1312-9.
40. Teuwen CP, Yaksh A, Lanters EA, Kik C, van der Does LJ, Knops P, et al. Relevance of Conduction Disorders in Bachmann's Bundle During Sinus Rhythm in Humans. Circ Arrhythm Electrophysiol. 2016;9(5):e003972.
41. Kharbanda RK, Knops P, van der Does L, Kik C, Taverne Y, Roos-Serote MC, et al. Simultaneous Endo-Epicardial Mapping of the Human Right Atrium: Unraveling Atrial Excitation. J Am Heart Assoc. 2020;9(17):e017069.
42. Mouws EMJP, van der Does LJME, Kik C, Lanters EAH, Teuwen CP, Knops P, et al. Impact of the arrhythmogenic potential of long lines of conduction slowing at the pulmonary vein area. Heart Rhythm. 2019;16(4):511-9.
43. Veeraraghavan R, Gourdie RG, Poelzing S. Mechanisms of cardiac conduction: a history of revisions. Am J Physiol Heart Circ Physiol. 2014;306(5):H619-H27.
44. Gray RA, Mashburn DN, Sidorov VY, Wikswo JP. Quantification of transmembrane currents during action potential propagation in the heart. Biophys J. 2013;104(1):268-78.
45. Sperelakis N, Hoshiko T. Electrical impedance of cardiac muscle. Circ Res. 1961;9:1280-3.
46. Houben RP, de Groot NM, Smeets JL, Becker AE, Lindemans FW, Allessie MA. S-wave predominance of epicardial electrograms during atrial fibrillation in humans: indirect evidence for a role of the thin subepicardial layer. Heart Rhythm. 2004;1(6):639-47.
47. Krogh-Madsen T, Abbott GW, Christini DJ. Effects of electrical and structural remodeling on atrial fibrillation maintenance: a simulation study. PLoS Comput Biol. 2012;8(2):e1002390-e.

48. Colman MA, Aslanidi OV, Kharche S, Boyett MR, Garratt C, Hancox JC, et al. Pro-arrhythmogenic effects of atrial fibrillation-induced electrical remodelling: insights from the three-dimensional virtual human atria. J Physiol. 2013;591(17):4249-72.
49. Fozzard HA, Schoenberg M. Strength-duration curves in cardiac Purkinje fibres: effects of liminal length and charge distribution. J Physiol. 1972;226(3):593-618.
50. van Campenhout MJH, Yaksh A, Kik C, de Jaegere PP, Ho SY, Allessie MA, et al. Bachmann's Bundle. Circulation: Arrhythmia and Electrophysiology. 2013;6(5):1041-6.
51. Zhou B. Sinoatrial node pacemaker cells: cardiomyocyte- or neuron-like cells? Protein & Cell. 2021;12(7):518-9.
52. Czick M, Shapter C, Silverman D. Atrial Fibrillation: The Science behind Its Defiance. Aging and Disease. 2016;7:635-56.
53. Wang K, Ho SY, Gibson DG, Anderson RH. Architecture of atrial musculature in humans. Br Heart J. 1995;73(6):559-65.
54. Siew Yen H, José Angel C, Damian S-Q. Left Atrial Anatomy Revisited. Circulation: Arrhythmia and Electrophysiology. 2012;5(1):220-8.
55. Cabo C, Pertsov AM, Baxter WT, Davidenko JM, Gray RA, Jalife J. Wave-front curvature as a cause of slow conduction and block in isolated cardiac muscle. Circ Res. 1994;75(6):1014-28.
56. Rolf S, Kircher S, Arya A, Eitel C, Sommer P, Richter S, et al. Tailored atrial substrate modification based on low-voltage areas in catheter ablation of atrial fibrillation. Circ Arrhythm Electrophysiol. 2014;7(5):825-33.
57. Anné W, Willems R, Roskams T, Sergeant P, Herijgers P, Holemans P, et al. Matrix metalloproteinases and atrial remodeling in patients with mitral valve disease and atrial fibrillation. Cardiovasc Res. 2005;67(4):655-66.
58. Elira M, Berend EW, Martin U, Dirk WD, Marcus C, Michael B. Cardiac remodeling in aortic and mitral valve disease: a simulation study with clinical validation. Journal of Applied Physiology. 2019;126(5):1377-89.
59. Voigt N, Dobrev D. Ion Channel Remodelling in Atrial Fibrillation. European Cardiology Review. 2011;7:97.
60. Nattel S, Maguy A, Le Bouter S, Yeh YH. Arrhythmogenic ion-channel remodeling in the heart: heart failure, myocardial infarction, and atrial fibrillation. Physiol Rev. 2007;87(2):425-56.
61. de Groot N, van der Does L, Yaksh A, Lanters E, Teuwen C, Knops P, et al. Direct Proof of Endo-Epicardial Asynchrony of the Atrial Wall During Atrial Fibrillation in Humans. Circulation: Arrhythmia and Electrophysiology. 2016;9(5):e003648.
62. Dhein S, Seidel T, Salameh A, Jozwiak J, Hagen A, Kostelka M, et al. Remodeling of cardiac passive electrical properties and susceptibility to ventricular and atrial arrhythmias. Frontiers in Physiology. 2014;5(424).
63. Spach MS, Miller WT, Geselowitz DB, Barr RC, Kootsey JM, Johnson EA. The discontinuous nature of propagation in normal canine cardiac muscle. Evidence for recurrent discontinuities of intracellular resistance that affect the membrane currents. Circulation Research. 1981;48(1):39-54.
64. Whitaker J, Rajani R, Chubb H, Gabrawi M, Varela M, Wright M, et al. The role of myocardial wall thickness in atrial arrhythmogenesis. Europace : European pacing, arrhythmias, and cardiac electrophysiology : journal of the working groups on cardiac pacing, arrhythmias, and cardiac cellular electrophysiology of the European Society of Cardiology. 2016;18(12):1758-72.

Appendix

Section A1: Description of the Python algorithm

The algorithm was created in normal SR. EA was determined in iterations for each U-EGM of an electrode channel. The baseline was determined using fixed window of 100 ms around the current LAT, given that the current LAT > 0 ms. Per EGM, excluding the first one, a baseline was extracted according to the interval $LAT - 100\ ms$ to $LAT - 30\ ms$. This baseline was low-pass filtered (< 1 Hz) using a first order Butterworth filter. The baseline was then interpolated through the EGM. The epicardial signal was corrected for baseline wander by subtracting the established baseline from it. This process was repeated for each EGM, and a final error margin was determined as the standard error of the mean (SEM) of the derivative of the entire epicardial signal. Limits of integration were then determined as crossings between baseline and epicardial signal using a fixed window of 50 ms around the current LAT, excluding the LAT itself. The area was then determined via trapezoidal integration. The results of the first analyzation are visualized in Figure 1.

Figure A1

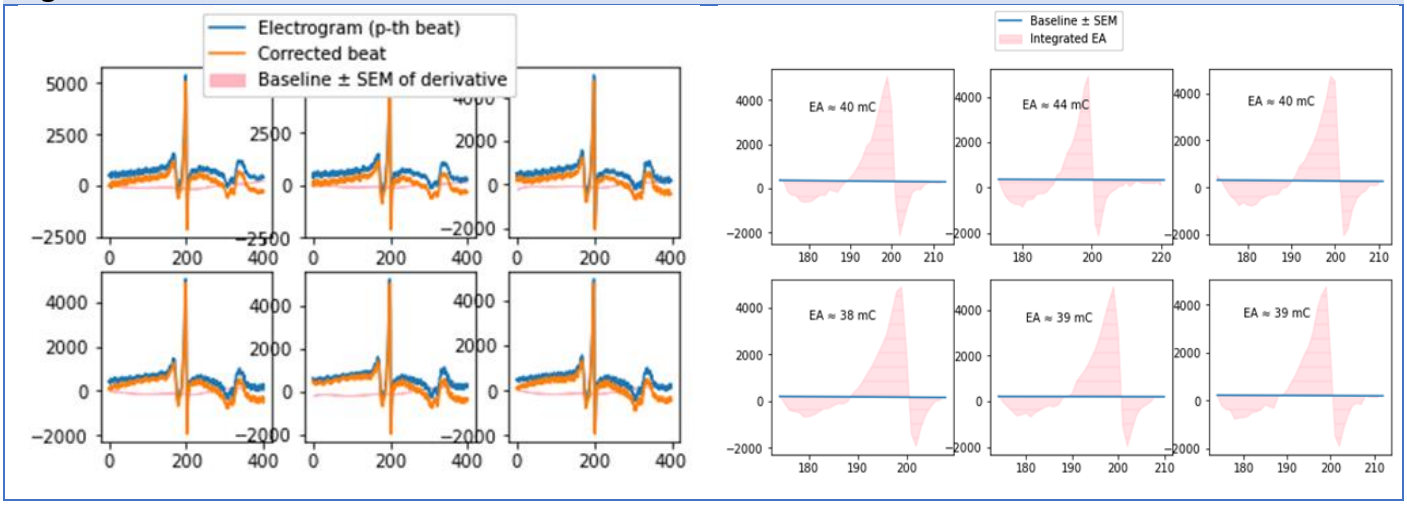

Representative examples of the epicardial signal, corrected signal and the established baseline with an error margin for a number of U-EGMs (left panel) and their resulting EAs (right panel) from a single patient.

The algorithm was then adapted to AF (Fig. 2) and fine-tuned to account for fractionation and remainders of baseline wander. The algorithm was fine-tuned, first by improving baseline through additional low-pass filtering and extracting its mean. Furthermore, R- and S-peak detection was implemented. The R-peak was defined as the first maximum value preceding the current LAT, while the S-peak was defined as the last minimum vale following the current LAT. The limits of integration were found using a fixed window of 50 ms around the current LAT. The starting point of the U-EGM and the first limit of integration is the crossing between epicardial signal and baseline + SEM before the R-peak. The endpoint of the U-EGM and the second limit of integration is the crossing between epicardial signal and baseline – SEM after the S-peak. In case of no crossings due to remaining baseline wander, the nearest values were used instead. For that scenario, a function was written yielding the smallest distance between two points.

Calculations of EA improved tremendously, but were distorted by far-field ventricular potentials. In a final step, the far-field potentials were therefore also cut from the epicardial signal when determining baseline. This removed remaining fluctuations and wander in the baseline. In addition, far-field ventricular potentials were not included in the EA. In case a LAT coincided with a far-field ventricular potential it was discarded from EA calculations. Furthermore, if far-field potentials occurred within the area of the U-EGM the limits of integration were adapted to the points before intrusion of the far-field potentials. Following the

finalization of the algorithm, values of EA were projected onto the electrode array to reveal the spatial distribution (Fig.3). Extra calculations were performed to derive the mean EA, variance and total EA. For the total EA, it was further decided to cut the 10 s AF recordings into two equal parts of 5 seconds to ensure equal comparison with SR recordings, which last 5 s by default.

Figure A2

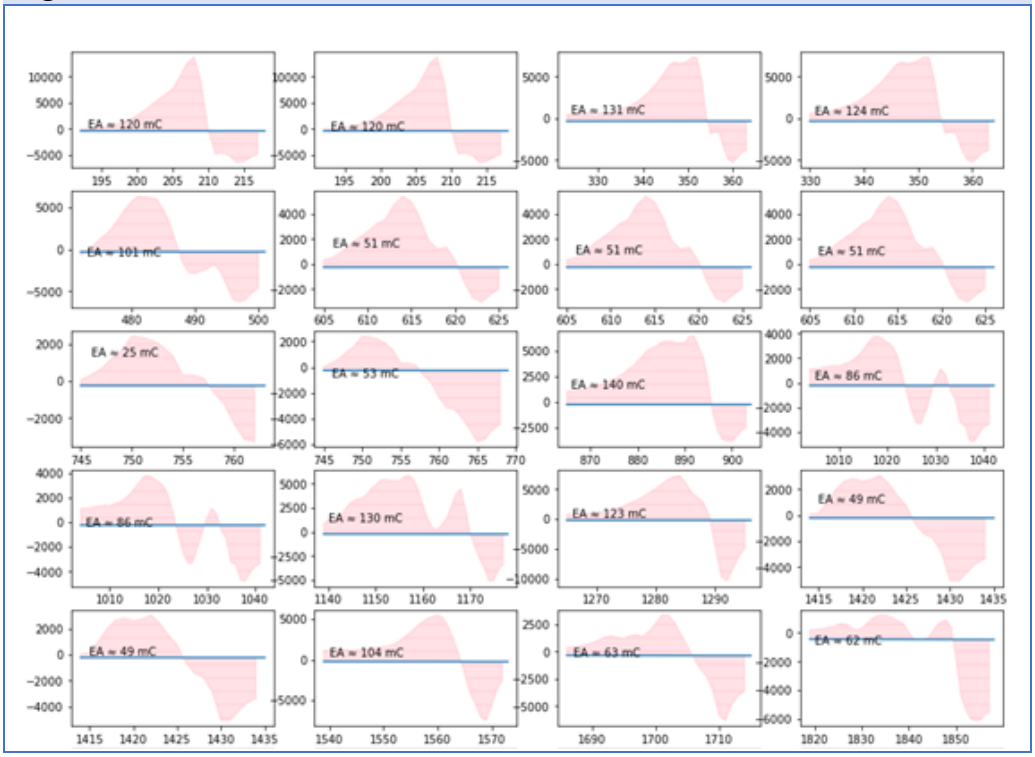

Representative examples of the derived EAs for a number of U-EGMs from a single patient.

Figure A3

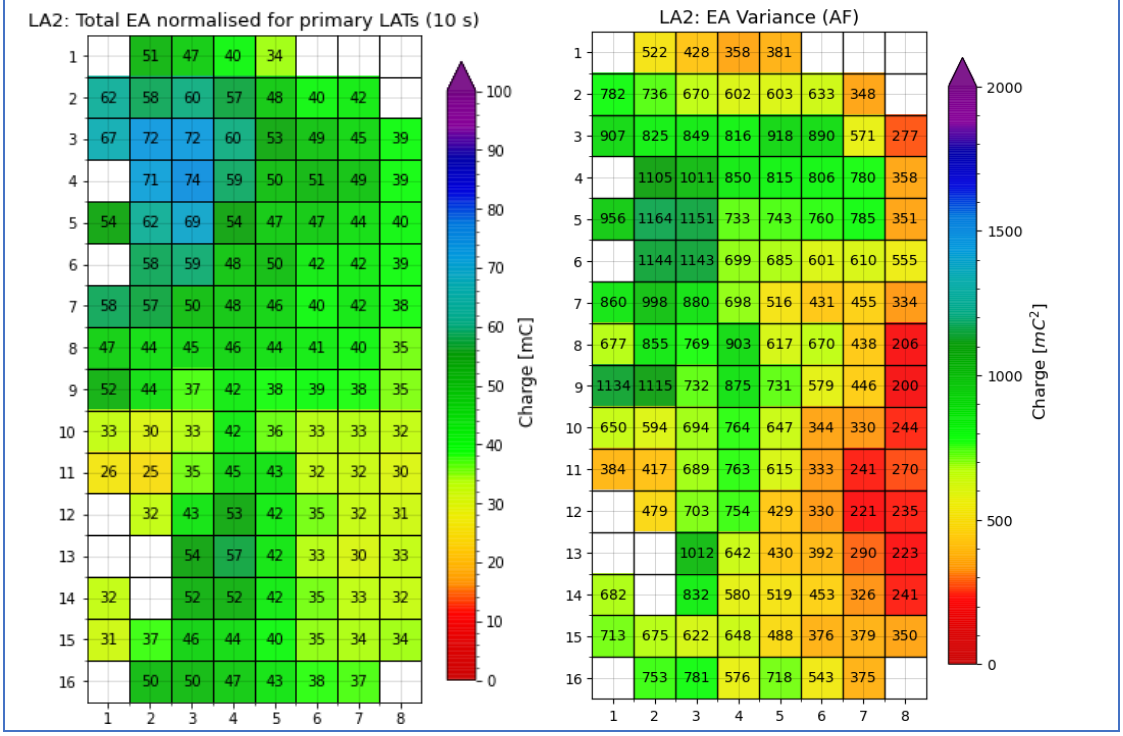

Representative examples of mean EA and EA variance projected onto the electrode array to reveal the spatial distribution.

Section A2: Additional Figures

Figure A4

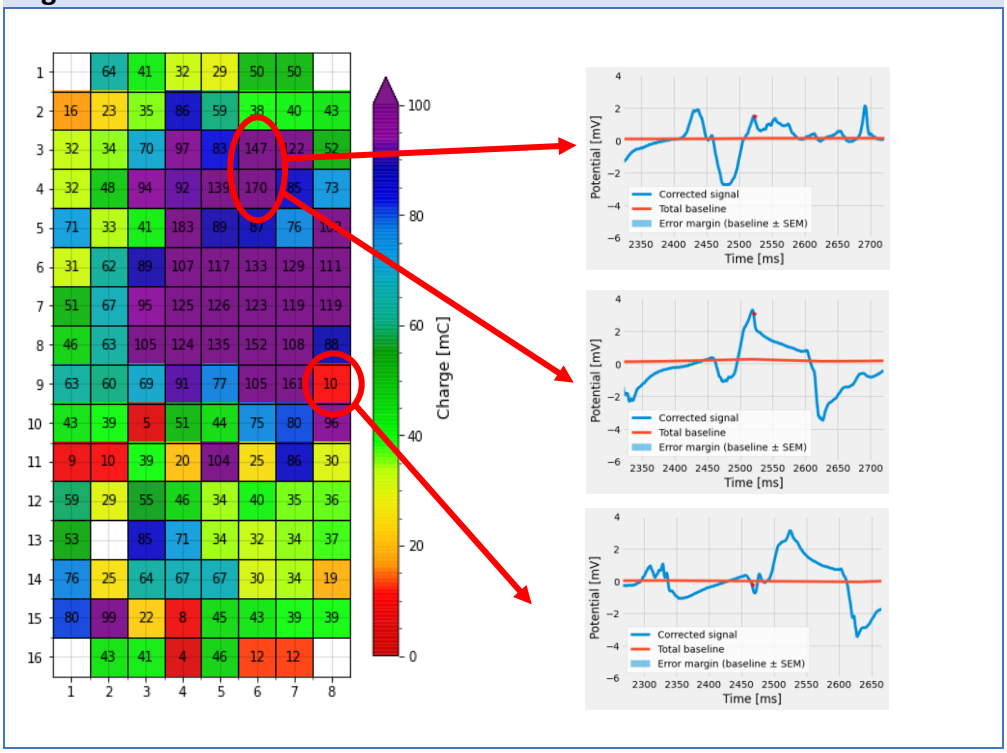

Representative example of U-EGM signal morphologies unipolar epicardial EA during AF for a random primary LAT, and the corresponding U-EGM morphologies for given EAs.

Figure 14

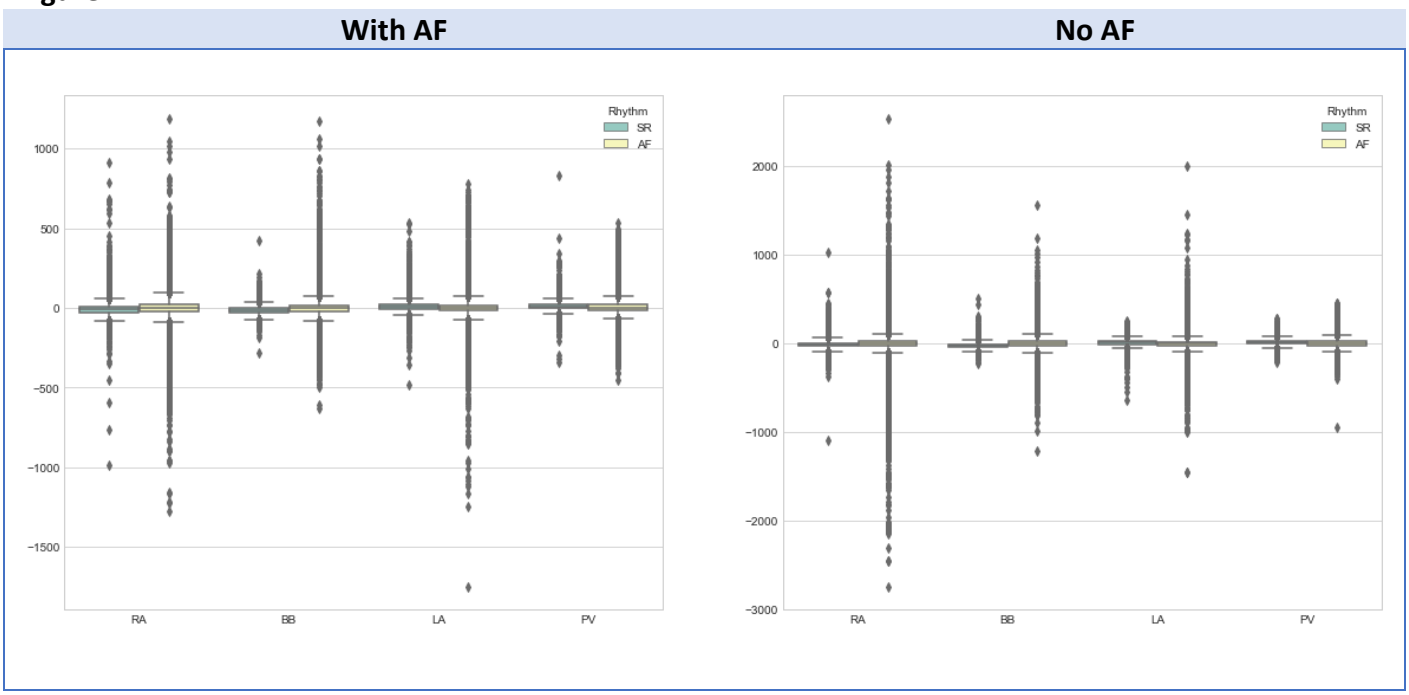

Boxplots with outliers of net EA across all atrial regions in the AF (left) and no AF group (right).